# Dalton Transactions

Accepted Manuscript






ROYAL SOCIETY OF CHEMISTRY

www.rsc.org/dalton

Cite this: DOI: 10.1039/c0xx00000x

www.rsc.org/xxxxxx

ARTICLE TYPE

# Towards better understanding of magnetic exchange mediated by hydrogen bonds in Mn(III)/Fe(III) salen-type supramolecular dimers

**Ivan Nemec, Radovan Herchel, Tomáš Šilha, and Zdeněk Trávníček***

***Received (in XXX, XXX) Xth XXXXXXXXX 20XX, Accepted Xth XXXXXXXXX 20XX***

**DOI: 10.1039/b000000x**

The thorough study of structural and magnetic properties were performed on a series of trinuclear and dinuclear M(III)/Fe(III) complexes consisting of $[M(L4)(Solv)]^{+}$ and $[Fe(CN)_5(NO)]^{2-}$ moieties (M = Fe(III) or Mn(III), Solv = $H_2O$ or $CH_3OH$, L4 = tetradentate salen-type ligands), in which dominant magnetic exchange is mediated by $O_S$–H···$O_{Ph}$ hydrogen bonds in $[M(L4)(Solv)]^{+}\cdots[M(L4)(Solv)]^{+}$ supramolecular dimers. As deduced from magnetic analysis involving also determination of zero-field splitting (ZFS) parameters for Mn(III) and Fe(III) ion as well as from comprehensive DFT calculations and modelling, it may be concluded that the strength of magnetic exchange is correlated with a number of hydrogen bonds and with the $O_{Ph}\cdots O_S$ distance between the phenolic oxygen of salen-type ligand ($O_{Ph}$) and oxygen of the solvent coordinated to the adjacent metal atom ($O_S$)

## Introduction

In recent years, significant amount of the research work has been devoted to the study of molecular magnetic materials due to their potential applications as molecular switches or high-density memory materials.[1] There is an unceasing effort to correlate magnetic properties of such materials to their structures in order to establish the rational design methods for preparation of molecule based magnetic materials. The most of the correlations dealt with the strength of the isotropic magnetic interactions mediated through the covalent bonds between two paramagnetic metal atoms,[2] or with the magnetic anisotropy defined by the zero-field splitting (ZFS) parameters – the prerequisite for observation of the slow-relaxation of magnetisation. However, there is another magnetic exchange coupling phenomenon emerging especially in the study of the organic-based molecular magnets and that is magnetic exchange mediated by non-covalent contacts such as hydrogen bonding or $\pi$–$\pi$ stacking of the aromatic rings. This kind of exchange might play important role also in the coordination compounds with interesting magnetic properties, *e.g.* in mediating intrachain exchange interaction thus giving rise to single-chain magnets,[3] in magnetic sponges,[4] in occurrence of slow-magnetic relaxation in polynuclear compounds[5] or in magnetic properties of simple paramagnetic compounds.[6]

The big group of the magnetically interesting coordination compounds are the cyanido-bridged complexes (so called Prussian blue analogues and related compounds) [7,8] which are of interest due to their structural and magnetic properties[9] or their potential use as optical devices and catalyst.[10] As a bridging unit a wide variety of the cyanido complexes can be used and these can be generally divided into two subgroups: **a)** homoleptic cyanido complexes with the general formula $[M(CN)_x]^{(x-m)-}$ (M = a transitional metal, $x$ = a number of cyanido ligands, $m$ = charge of M), and **b)** heteroleptic cyanido complexes $[M(L)(CN)_x]^{(x+l-m)-}$ (L = an organic ligand different from CN, $l$ = charge of L). Such cyanidometallates can be left further to react with the coordinatively unsaturated complexes (or with labile complexes from the kinetic point of view) forming thus compounds exhibiting a wide variability in their structures and magnetic properties.

The objective of this article was to prepare and characterize a series of trinuclear nitroprusside bridged Mn(III)/Fe(III) complexes containing Schiff base ligands[11], more concretelly, salen-type ligands ($L4^{2-}$ = salen$^{2-}$ = *N*,*N*'-ethane-bis(salicylideneiminate) dianion, other abbreviations of the ligands used or mentioned in this work can be found in the reference[12]) and therefore, such type of polynuclear salen-type compounds bridged by metallocyanate will be discussed below briefly.

The cationic part in the presented complexes consists of the tetradentate salen-like dianion ligand ($L4^{2-}$) coordinated to the transition metal creating thus the $[M(L4)]^{(m-2)-}$ moiety with the L4 ligand forming the equatorial plane of the complex. Two axial positions are potentially available for the coordination and therefore, the $[M(L4)]^{(m-2)-}$ moiety can be considered as a perfect building block for the preparation of low dimensional coordination compounds but also variously dimensional (1D, 2D or 3D) coordination polymers can be prepared. In general, three basic structural types can be distinguished where the $[M(L4)]^{(m-2)-}$ moiety is coordinated by:

**a)** One *N*-cyanido ligand from the cyanidometallate and the second axial position is occupied by the solvent molecule (most usually water or methanol). The resulting complex structure is low-dimensional and polynuclear due to the terminal function of the solvent ligand (further abbreviated as Solv). However, the

Solv molecules often extend the dimensionality (usually to 1D arrays) of the crystal structure by the hydrogen bonding formed with suitable acceptor atoms from the neighbouring molecules (Scheme 1A, *vide infra*).

**b)** Two *N*-cyanido ligands, each from different adjacent cyanidometallate molecules and therefore, the resulting complex structure is polymeric in most cases (Scheme 1B, *vide infra*).

**c)** One *N*-cyanido ligand from the cyanidometallate whereas the second position is occupied by the phenolic oxygen atom from the adjacent $[M(L4)]^{(m-2)-}$ molecule forming thus the dimeric unit. It must be stressed that this kind of the dimer is not unique for the $Mn^{III}$ complexes only, but it can be also found in other transition metal complexes ($Co^{II/III}$,[13] $Fe^{III}$,[14] $Ru^{III}$,[15] $Ti^{III}$,[16] $Zn^{II}$,[17] $Cu^{II}$ [18] and $Ni^{II}$ [19], Scheme 1C).

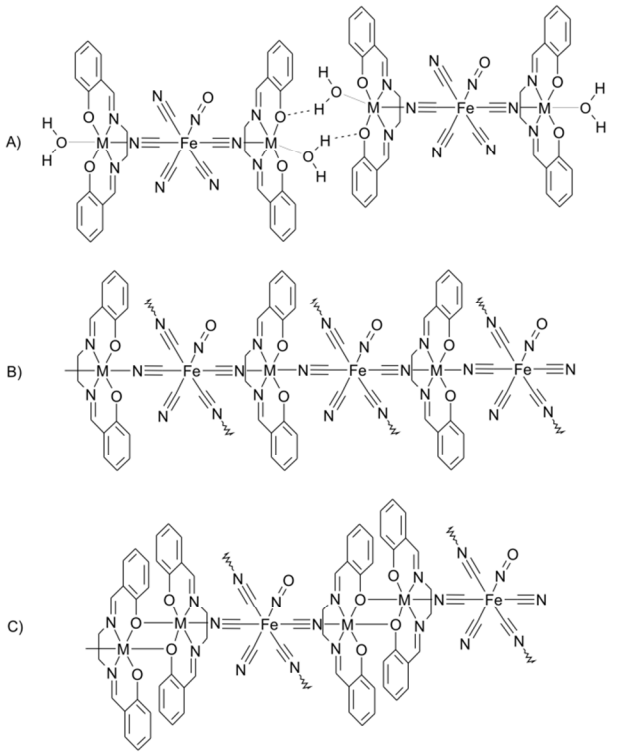


**Scheme 1.** Schematic representations of three structural types of the $[M(L4)]^{(m-2)-}$ complexes with cyanidometallates

In our previous works we have reported on the coordination compounds built from various $[Mn^{III}(L4)]^+$ moieties bridged by the $[Pt(SCN)_4]^{2-}$ or $[Pt(SCN)_6]^{2-}$ complex anions.[20,21] Almost all of the prepared compounds were trinuclear with the general formula $[\{Mn(L4)(Solv)\}_2\{\mu\text{-}Pt(SCN)_x\}]$, where $x$ = 4 or 6, and thus they belong to the group (a). It was shown that the exchange interactions mediated by the diamagnetic bridging anion are negligible and it was proved that the dominant magnetic exchange pathway is included by non-covalent interactions, i.e. hydrogen bonding within the supramolecular dimer $[Mn(L4)(Solv)]^+\cdots[Mn(L4)(Solv)]^+$. Therefore, this kind of supramolecular system represents an ideal object of study for investigation of the magnetic exchange mediation through hydrogen bonding. Furthermore, it was observed that there is a significant difference in the strength of the magnetic exchange depending from the type of the Solv molecule bonded to the $Mn^{III}$ atom. In order to explore this phenomenon thoroughly we have decided to study another system with diamagnetic bridging cyanidometallate, i.e. nitroprusside $[Fe(CN)_5(NO)]^{2-}$ and further, we have focused our attention not only to its $Mn^{III}$ complexes but also to the $Fe^{III}$ ones.

From the literature survey aimed on the above mentioned compounds it is apparent that the nitropusside–$[M^{III}(L4)]^+$ compounds ($M^{III}$ = $Fe^{III}$, $Mn^{III}$), which belong to group (A, Scheme 1A) involve only $Mn^{III}$ complexes (the explanation of the ligand abbreviations can be found in Scheme 2): $[\{Mn(L4i)(H_2O)\}_2\{\mu\text{-}Fe(CN)_5(NO)\}]$ (**7a**),[22] $[\{Mn(L4b)(H_2O)\}_2\{\mu\text{-}Fe(CN)_5NO\}]\cdot 2CH_3OH$ (**7b**), $[\{Mn(L4m)(CH_3OH)\}_2\{\mu\text{-}Fe(CN)_5NO\}]$ (**7c**),[23] $[\{Mn(L4k)(H_2O)\}_2\{\mu\text{-}Fe(CN)_5NO\}]\cdot 2H_2O$ (**7d**) [24] and $[\{Mn(L4l)(H_2O)\}_2\{\mu\text{-}Fe(CN)_5NO\}]$ (**7e**).[25]

The compounds of the group (B) are polymeric with two-dimensional crystal structure (Scheme 1B). The nitroprusside anion acts as a moiety bridging four $[M^{III}(L4)]^+$ entities in all the reported cases, and creating thus the grid-like sheets built from the $[\{M(L4)\}_2\{\mu_4\text{-}Fe(CN)_5NO\}]_n$ units. This group contains six coordination polymers: $[\{Mn(L4j)\}_2\{\mu_4\text{-}Fe(CN)_5(NO)\}]$ (**7f**) [26], $[\{Mn(L4f)\}_2\{\mu_4\text{-}Fe(CN)_5(NO)\}]$ (**7g**) [24], $[\{Fe(L4f)\}_2\{\mu_4\text{-}Fe(CN)_5(NO)\}]_n$ (**7h**) [27], $[\{Fe(L4g)\}_2\{\mu_4\text{-}Fe(CN)_5(NO)\}]$ (**7i**) [28], $[\{Mn(L4f)\}_2\{\mu_4\text{-}Fe(CN)_5(NO)\}]\cdot 2H_2O$ (**7j**) 2 and $[\{Mn(L4f)\}_2\{\mu_4\text{-}Fe(CN)_5(NO)\}]\cdot 2H_2O$ (**7k**) [23].

The group (C), depicted in Scheme 1C, is represented by one example only: $[\{Mn(L4h)\}_2\{\mu_4\text{-}Fe(CN)_5(NO)\}]$ (**7l**).[24] This compound is polymeric with four $[\{Mn(L4h)\}_2]^{2+}$ dimers bridged by one nitroprusside anion thus creating two-dimensional network. In this article the great deal of attention is devoted to the study of seven novel trinuclear nitroprusside complexes with salen-type Schiff base ligands having the general formula $[\{M^{III}(L4)(H_2O)\}_2\{\mu\text{-}Fe(CN)_5(NO)\}]\cdot x CH_3OH$, $x$ = 0 or 1 and M = Fe or Mn.

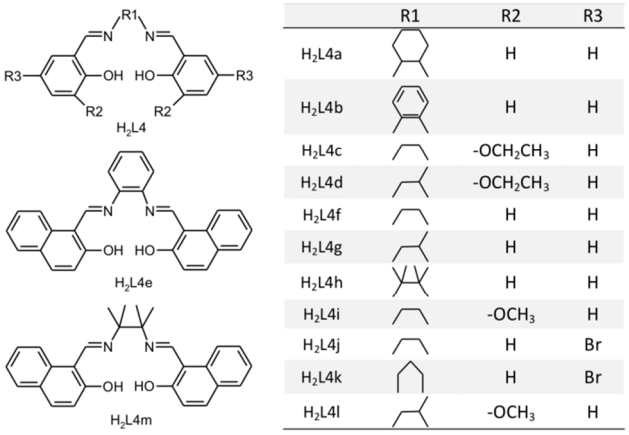


| | R1 | R2 | R3 |
|---|---|---|---|
| $H_2L4a$ | | H | H |
| $H_2L4b$ | | H | H |
| $H_2L4c$ | | $-OCH_2CH_3$ | H |
| $H_2L4d$ | | $-OCH_2CH_3$ | H |
| $H_2L4f$ | | H | H |
| $H_2L4g$ | | H | H |
| $H_2L4h$ | | H | H |
| $H_2L4i$ | | $-OCH_3$ | H |
| $H_2L4j$ | | H | Br |
| $H_2L4k$ | | H | Br |
| $H_2L4l$ | | $-OCH_3$ | H |

**Scheme 2.** Schematic representations of $H_2L4$ tetradentate Schiff base ligands used in this work and their abbreviations.

The crystal structures of the complexes $[\{Fe(L4b)(H_2O)\}_2\{\mu\text{-}Fe(CN)_5(NO)\}]\cdot 2CH_3OH$ (**3a**), $[\{Fe(L4c)(H_2O)\}_2\{\mu\text{-}Fe(CN)_5(NO)\}]$ (**4a**), $[\{Mn(L4c)(H_2O)\}_2\{\mu\text{-}Fe(CN)_5(NO)\}]$ (**4b**) and $[\{Fe(L4d)(H_2O)\}_2\{\mu\text{-}Fe(CN)_5(NO)\}]$ (**5a**) have been determined by a single X-ray diffraction. The magnetic measurements were performed for all the prepared compounds including two

compounds without determined crystal structures: $[\{Fe(L4a)(H_2O)\}_2\{\mu\text{-}Fe(CN)_5(NO)\}]\cdot CH_3OH$ (**2a**), $[\{Mn(L4a)(H_2O)\}_2\{\mu\text{-}Fe(CN)_5(NO)\}]\cdot CH_3OH$ (**2b**). Furthermore, we report on novel type of the nitroprusside complex with ionic structure where the $[\{Mn(L4e)(H_2O)\}\{\mu\text{-}Fe(CN)_5(NO)\}]^-$ anion is charge balanced by the $[\{Mn(L4e)(H_2O)(CH_3OH)\}]^+$ cation (**6b**).

With the aim to elucidate the magnetic exchange and magnetic anisotropy in herein reported compounds, temperature and field dependent magnetic data were simultaneously fitted to provide trustworthy values of isotropic exchange constants ($J$) and single-ion zero-field splitting parameters ($D$). Furthermore, thorough DFT study was undertaken to determine dominant super-exchange pathways and the role of minor changes in crystal structures on overall magnetic exchange. Ultimate goal of our investigations is to build up a magneto-structural correlation between the isotropic magnetic exchange constant $J$ and structural parameters in the group of compounds containing $[M(L4)(Solv)]^+\cdots[M(L4)(Solv)]^+$ supramolecular dimers. So far several studies devoted to magnetic exchange mediated by O–H···O hydrogen bonds were published,[29] but mainly for copper(II) complexes, in which only the isotropic exchange is present. In our study, the situation is complicated by zero-field splitting of Fe(III) and Mn(III) atoms, and thus, advanced magnetic analysis had to be employed.

## Results and Discussion

### Crystal structures of trinuclear complexes 3a, 4a, 4b and 5a

The selected bond lengths for herein and already reported salen-type complexes are summarized in Table 1. The crystal data and structure refinements for compounds reported in this article are given in Table 2.

The molecular structures of these complexes are very similar consisting of the trinuclear $[\{M^{III}(L4)(H_2O)\}_2\{\mu\text{-}Fe(CN)_5(NO)\}]$ moieties ($M^{III}$ = $Fe^{III}$ or $Mn^{III}$, Fig. S1-S4 in Electronic Supplementary Information (ESI)), which have slightly bent $\{H_2O\text{-}M^{III}\text{-}NC\text{-}Fe\text{-}CN\text{-}M^{III}\text{-}H_2O\}$ arrangement, (Fig. 1-3). The $M^{III}\cdots M^{III}$ separations within the trinuclear complexes are very similar (in Å): 10.1621(6) in **3a**, 10.1532(5) in **4a**, 10.225(2) in **4b** and 10.173(4) in **5a**. The coordination polyhedrons of the $[M(L4)(H_2O)]^+$ subunits can be described as axially elongated octahedrons and the distortion is more obvious for the Mn(III) derivatives due to the Jahn-Teller effect. In general, it can be concluded, as for herein and previously reported salen-type complexes, that the Mn(III) compounds show significantly longer axial (usually M-$N_{CN}$ and M-$O_S$ bonds, $N_{CN}$ stands for nitrogen atom of the nitroprusside cyanido group, $O_S$ is oxygen atom from coordinated solvent molecule) bond lengths (*ca*. $d$(Mn-$N_{CN}$) = 2.30 Å, $d$(Fe-$N_{CN}$) = 2.17 Å, $d$(Mn-$O_S$) = 2.27 Å, $d$(Fe-$O_S$) = 2.10 Å, Table 1) in comparison with Fe(III) ones. On the contrary, the M-$N_{im}$ bond lengths are longer in the case of the Fe(III) complexes (*ca*. $d$(Mn-$N_{im}$) = 1.99 Å, $d$(Fe-$N_{im}$) = 2.11 Å, $N_{im}$ stands for nitrogen atom from imino group of L4). The length of the M-$O_{Ph}$ bonds is roughly the same for both central ions (Table 1, $O_{Ph}$ stands for the phenolate oxygen atoms). The angular distortions from the ideal octahedron $\Sigma$[30] are obviously smaller for the Mn(III) compounds (Table 1).

As it was mentioned in the introduction these trinuclear complexes belong to the group (a) in which the non-covalent connections between the polynuclear species are provided by the hydrogen bonding between the coordinated Solv molecules and phenolate oxygen atoms and thus, the roughly linear arrays of the centrosymmetric and supramolecular $[Mn(L4)(Solv)]^+\cdots\cdots[Mn(L4)(Solv)]^+$ dimers "separated" by the nitroprusside anions are formed. In the crystal structure of the compounds **3a**, **4a**, **4b** and **5a** the Solv molecules (Solv = $H_2O$) form two basic types of the interconnections: i) simple $O_S$–H···$O_S$ hydrogen bond (in **3a**), ii) bifurcated hydrogen bond where two H-atoms from the water molecule interact with four oxygen atom acceptors (two alkoxy ($O_A$) and two phenolate oxygen atoms, in **4a**, **4b** and **5a**). The hydrogen bonding bifurcation prolongs the donor···acceptor lengths in the case of $O_S\cdots O_{Ph}$ contacts (in Å): $d$($O_S\cdots O_{Ph}$) = 2.690(3) in **3a** vs. 2.792(2) and 2.927(2) in **4a**, 2.851(3) and 2.934(3) in **4b**, 2.814(2) and 2.866(2) in **5a**. The $O_S\cdots O_A$ hydrogen bonds are longer in general, however, in crystal structure of **4b** we observe one relatively short contact (in Å): $d$($O_S\cdots O_A$) = 3.024(2) and 3.248(2) in **4a**, 2.866(3) and 3.115(4) in **4b**, 3.064(2) and 3.279(2) in **5a**.

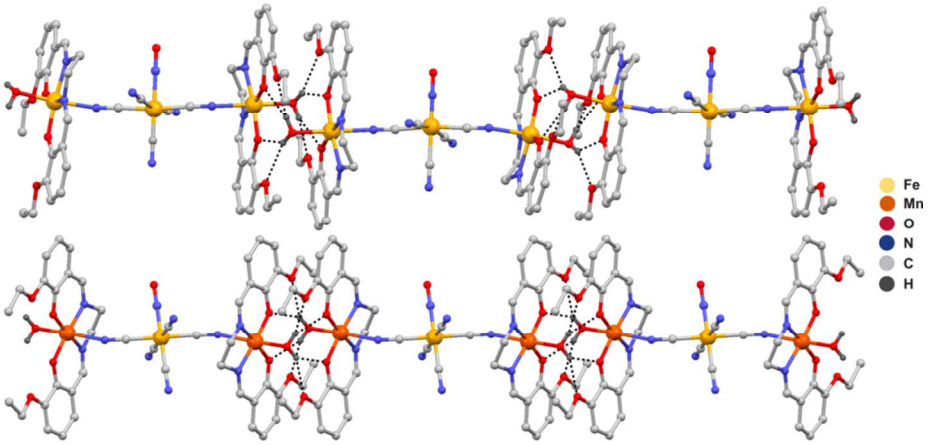


**Fig. 1** Fragments of the crystal structures of the complexes **4a** (up) and **4b** (down). The hydrogen atoms are omitted for clarity, except for the atoms responsible for the formation of "supramolecular dimer" of **4a** and **4b** due to hydrogen bonds (dashed lines). Selected bond lengths and angles are shown in Figs. S2 and S3 in ESI.

Cite this: DOI: 10.1039/c0xx00000x

www.rsc.org/xxxxxx

# ARTICLE TYPE

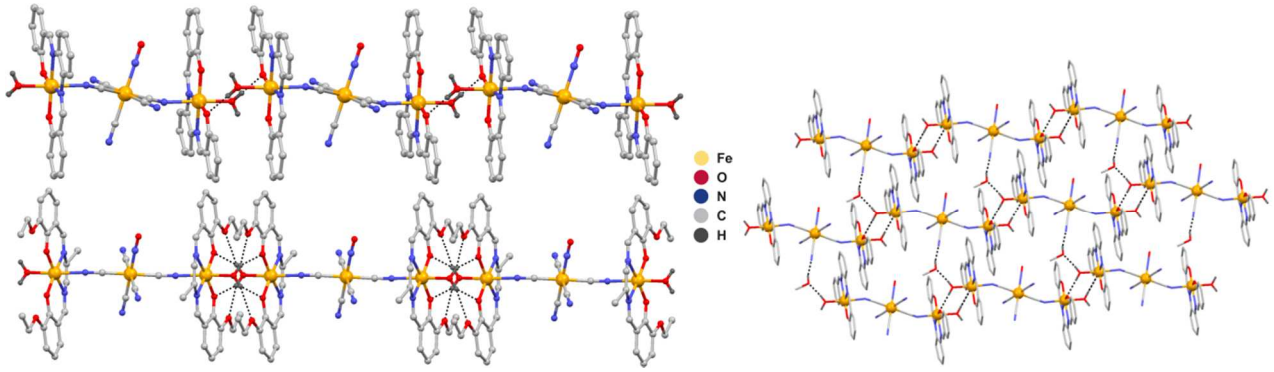


**Fig. 2** Left: Fragments of the crystal structures of the complexes **3a** (left up) and **5a** (left down). The hydrogen atoms and methanol molecules (**3a**) are omitted for clarity, except for the atoms responsible for the formation of "supramolecular dimer" of **3a** and **5a** due to hydrogen bonds (dashed lines). Selected bond lengths and angles are shown in Figs S1 and S4 in ESI. Right: A perspective view on the 2D supramolecular structure in **3a**.

The $M^{III}\cdots M^{III}$ separations within the supramolecular dimer are from relatively narrow range (in Å): 4.8728(5) in **3a**, 4.5608(4) in **4a**, 4.7132(9) in **4b** and 4.594(2) in **5a**. The crystal structure of **3a** differs significantly from the structures of **4a**, **4b** and **5a** due to a presence of the co-crystallized molecule of methanol. This extends the structural dimensionality of the compound to 2D by linking supramolecular chains $[\{Fe(L4b)(H_2O)\}_2\{\mu\text{-}Fe(CN)_5(NO)\}]_n$ together by hydrogen bonding between coordinated water molecule and methanol and further, methanol is hydrogen bonded to non-coordinated nitrogen atom from the neighbouring nitroprusside bridging complex (Fig. 2).

### Crystal structure of complex 6b

The crystal structure of **6b** is depicted in Fig. 3. It consists of the dimeric $[\{Mn(L4e)(H_2O)\}\{\mu\text{-}Fe(CN)_5NO\}]$ (**6b** mol1) and $[\{Mn(L4e)(H_2O)(CH_3OH)]$ (**6b** mol2) moieties, where both manganese atoms are hexacoordinated with four donor atoms ($N_2O_2$) coming from the $L4e^{2-}$ ligand. The remaining coordination sites (axial positions) are occupied by two oxygen atoms coming from the coordinated water and methanol in **6b** mol1, on the other hand, the axial positions in **6b** mol2 are occupied by the oxygen atom from the water molecule and by the nitrogen atom from the bridging cyanido group of nitroprusside. The average bond lengths are (mol1, mol2; in Å): $d(Mn–N_{im})$ = 1.961, 1.953, $d(Mn–O_{Ph})$ = 1.882, 1.868. The axial bond lengths differ in the length due to the different solvent molecule coordinated to the Mn(III) atom (in Å): $d(Mn\text{-}O_S)$ = 2.292(3) ($H_2O$) in mol1, 2.256(3) ($CH_3OH$) and 2.309(3) ($H_2O$) in mol2. It must be noted that the crystal structure of **6b** exhibits substitutional disorder on mol2, where the methanol molecule (the main part, the occupation factor of 0.68) is partially substituted by the water molecule and this is further hydrogen bonded to another disordered water molecule (Fig. S5 in ESI).

**Table 1** Selected structural parameters for nitroprusside complexes. Bond lengths are given in Å.

| | $M\text{-}N_{im}$[a] | $M\text{-}O_{Ph}$[a] | $M\text{-}N_{CN}$ | $M\text{-}O_S$ | $\Sigma°$[b] |
|---|---|---|---|---|---|
| **3a** | 2.109 | 1.896 | 2.151(2) | 2.0548(16) | 37.7 |
| **4a** | 2.085 | 1.897 | 2.1512(14) | 2.1309(12) | 56.4 |
| **4b** | 1.973 | 1.878 | 2.343(3) | 2.256(2) | 44.4 |
| **5a** | 2.084 | 1.889 | 2.163(2) | 2.143(2) | 53.9 |
| **6b mol1** | 1.962 | 1.882 | 2.245(3) | 2.292(2) | 22.4 |
| **6b mol2** | 1.953 | 1.868 | – | 2.309(2)<br>2.256(2) | 29.5 |
| **7a** | 1.970 | 1.863 | 2.355(6) | 2.271(5) | 49.6 |
| **7b** | 1.986 | 1.872 | 2.304(6) | 2.223(5) | 27.2 |
| **7c** | 1.962 | 1.881 | 2.288(4) | 2.358(3) | 53.8 |
| **7d** | 2.036 | 1.900 | 2.263(6) | 2.224(5) | 35.4 |
| **7e** | 1.981 | 1.880 | 2.394(2) | 2.258(2) | 46.3 |
| **7f** | 1.989 | 1.863 | 2.378(2) | – | 54.1 |
| **7g** | 1.985 | 1.888 | 2.305(3) | – | 34.1 |
| **7h** | 2.109 | 1.898 | 2.173(6) | – | 57.0 |
| **7i** | 2.111 | 1.898 | 2.175(5) | – | 55.3 |
| **7j** | 1.987 | 1.888 | 2.304(4) | – | 33.8 |
| **7k** | 1.969 | 1.881 | 2.326(3) | – | 35.9 |
| **7l** | 1.978 | 1.885 | 2.246(4) | – | 57.7 |

[a] The average values calculated from two bond length values. [b] Distortion parameter defined as sum of deviations from 90° of the twelve *cis* angles in the coordination sphere.[30]

Both complex molecules with an assistance of the co-crystallized water and methanol molecules create rich 2D network of hydrogen bonds (Fig. 3). As a main building block of the crystal structure the $[\{Mn(L4e)(H_2O)\}\{\mu\text{-}Fe(CN)_5NO\}][\{Mn(L4e)(H_2O)(CH_3OH)]$ assembly (mol1$\cdots$mol2) can be considered, in which the interconnection between the mol1 and mol2 parts is provided by hydrogen bonding between the coordinated water molecules and complementary phenolate oxygen atoms, similarly to compounds **3a**–**5a**. The mol1$\cdots$mol2 assembly is further propagated to linear 1D chain by a series of hydrogen bonds between the coordinated methanol molecule from mol2 and co-crystallized water molecule

and further by hydrogen bonding to co-crystallized methanol, which is in a close contact with the adjacent cyanido group (the *trans* position with respect to the cyanido group coordinating the Mn atom) from the other mol1···mol2 assembly. Linear supramolecular chains are interconnected via hydrogen bonding between the coordinated water molecule from the mol1 part and the neighbouring cyanido group (the *cis* position with respect to the cyanido group coordinating the Mn atom) and also by hydrogen bonds between the co-crystallized water molecule and cyanido group from the neighbouring mol1 moiety.

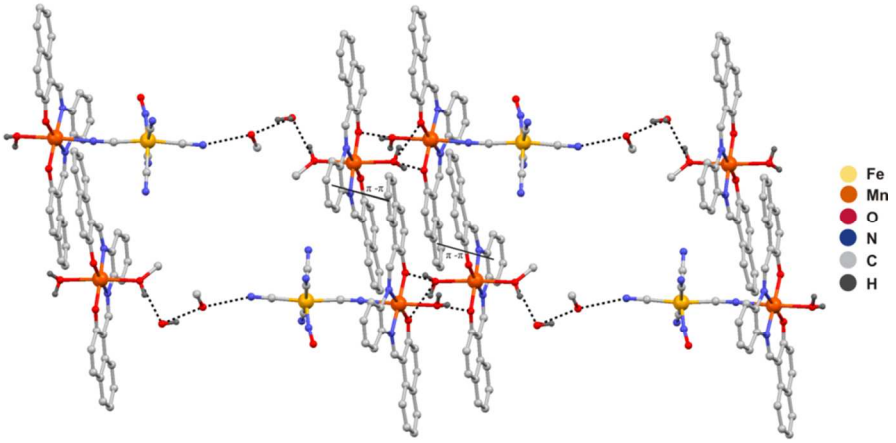


**Fig. 3**. Fragment of the crystal structure of the complex **6b**. The hydrogen atoms are omitted for clarity, except for the atoms responsible for the formation of "supramolecular dimer" of **6b** due to hydrogen bonds and highlight several $\pi$-$\pi$ stacking in the complex (dashed lines). Selected bond lengths (Å) and angles (°) are shown in Fig. S5 in ESI.

### Infrared spectroscopy

The presence of the Schiff base in the complexes was indicated by FT-IR spectra measured in the range of 400-4000 $cm^{-1}$. The spectra of all the compounds exhibit two weak intensity bands at 3115-3132 and 3025-3037 $cm^{-1}$ corresponding to asymmetric and symmetric stretching vibrations of the aromatic C–H groups. The characteristic bands assignable to the C=N and $(C–C)_{ar}$ vibrations were observed in the 1625-1613 $cm^{-1}$, and 1595-1437 $cm^{-1}$ region, respectively, in all complexes. Formations of the cyanido-bridges in all the nitroprusside complexes are evidenced by the C≡N vibration stretching bands in the 2000-2200 $cm^{-1}$ region. The maximum at 2143 $cm^{-1}$ may be assigned to the vibration of the cyanido group in sodium nitroprusside dihydrate, while the maxima associated with the vibration in the case of complexes **2a-6b** were observed in the range of 2138-2163 $cm^{-1}$.[31] The strong peaks in the region of 1906-1922 $cm^{-1}$ are assignable to the N=O stretching vibration, which is lower than that found in the complex $Na_2[Fe(CN)_5NO]·2H_2O$ (1936 $cm^{-1}$).

### Magnetic properties

In all the presented compounds, we can observe the formation of quasi-dimers among $[\{Mn^{III}(L4)(H_2O)\}]^+$ or $[\{F^{eIII}(L4)(H_2O)\}]^+$ subunits held by hydrogen bonds between the coordinated solvent molecules and phenolic oxygen atoms. Within these quasi-dimers, the Mn···Mn and Fe···Fe separations vary between 4.71-5.06 Å, and 4.59-4.87 Å, respectively, in contrast to large interatomic distances (more than 10 Å) through covalent bonds formed by diamagnetic nitroprusside bridges.

These structural aspects strongly suggest that the super-exchange mechanism is mainly active through hydrogen bonds. The nature of the magnetic exchange can be estimated by inspecting the temperature dependence of susceptibility and the effective magnetic moment of these compounds. The presence of the maximum on susceptibility ($T$ < 10 K) is a fingerprint of the antiferromagnetically coupled homospin dimer. This results in decrease of $\mu_{eff}/\mu_B$ on cooling. Moreover, the interplay of the zero-field splitting on magnetic properties cannot be neglected, especially for Mn(III) atoms.

Therefore the following spin Hamiltonian was postulated

$$\hat{H} = -J\left(\vec{S}_1 \cdot \vec{S}_2\right) + \sum_{i=1}^{2} D_i(\hat{S}_{i,z}^2 - \hat{S}_i^2/3) + \mu_B B g_i \hat{S}_{i,a} - zj\left\langle \hat{S}_{i,a} \right\rangle \hat{S}_{i,a} \quad (1)$$

The first term stands for the isotropic exchange ($J$), the second part is due to the zero-field splitting ($D$ – an axial single-ion ZFS parameter), the third part is the Zeeman term and the last expression represented with the $zj$ variable is the common molecular-field correction parameter, which is due to small intra/inter-chain molecular interactions. The $\langle S_a \rangle$ is a thermal average of the molecular spin projection in $a$ direction of magnetic field defined as $\mathbf{B}_a = B·(\sin\theta\cos\varphi, \sin\theta\sin\varphi, \cos\theta)$ with the help of the polar coordinates. Then, the molar magnetization in $a$-direction of magnetic field can be numerically calculated as

$$M_a = -N_A \frac{\sum_i \left( \sum_k \sum_l C_{ik}^{+} (Z_a)_{kl} C_{li} \right) \exp\left(-\varepsilon_{a,i}/kT\right)}{\sum_i \exp\left(-\varepsilon_{a,i}/kT\right)} \quad (2)$$

where Za is the matrix element of the Zeeman term for the a-direction of the magnetic field and C are the eigenvectors resulting from the diagonalization of the complete spin Hamiltonian matrix. Then, the averaged molar magnetization of the powder sample was calculated as integral (orientational) average

$$M_{mol} = 1/4\pi \int_0^{2\pi} \int_0^{\pi} M_a \sin\theta d\theta d\varphi \quad (3)$$

With the aim to bring more insight in general properties of the antiferomagnetically coupled dimer with ZFS, the shift of temperature of maximum of the susceptibility ($T_{max}$) was inspected for varying ratios of $D/J$ either for $S_1 = S_2 = 2$ or $S_1 = S_2$

= 5/2 (Fig. 4). There is a simple formula, which interconnects the strength of the antiferromagnetic exchange with $T_{max}$, but it is available only for the isotropic case: $|J|/kT_{max} = 0.462$ for $S_1 = S_2 = 2$ and $|J|/kT_{max} = 0.347$ for $S_1 = S_2 = 5/2$. In both cases, the introducing the non-zero zero-field splitting results in increase of $T_{max}$, and this change is more emphasized for $D < 0$ (Fig. 4).

As both antiferromagnetic exchange and ZFS have similar effects on magnetic properties, the decrease of the $\mu_{eff}/\mu_B$, the both temperature and field dependent magnetization data were experimentally acquired and concurrently used in finding the best-fit parameters of the above introduced spin Hamiltonian (eq.1). Furthermore, the standard deviations of varied parameters were calculated with 95% probability confidence limits.[32]

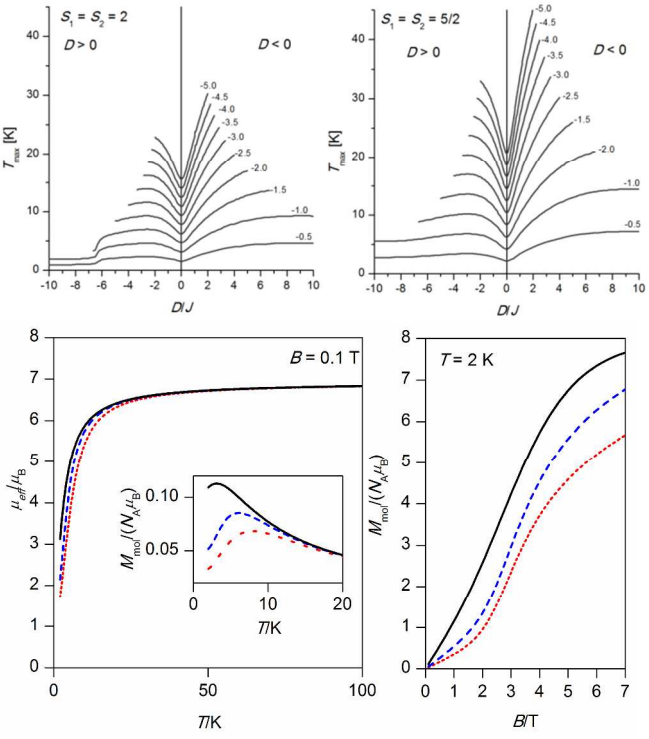


**Fig. 4** Top: the modelling of the interplay of the antiferromagnetic exchange ($J$) and the single-ion zero-field splitting ($D$) on the temperature of the maximum of the molar magnetization (or the mean susceptibility) $T_{max}$ for a dinuclear systems. The line's labels correspond to $J$'s values. The D-parameter was varied from -10 to +10 cm$^{-1}$. Bottom: the variation of magnetic properties for $S_1 = S_2 = 2$ dimer, with the fixed parameters $J$ = -1 cm$^{-1}$ and $g = 2.0$, while $D$ was varied: $D = 0$ (black full line), $D$ = -2 cm$^{-1}$ (blue dashed line) and $D$ = -4 cm$^{-1}$ (red dotted line).

## Dinuclear complex 6b

The unique molecular and crystal structure of **6b** results in forming quasi linear and discrete trimers of $Mn^{III}$-$Mn^{III}$-$Fe^{II}$ type in which paramagnetic manganese atoms are connected through hydrogen bonds ($d$(Mn···Mn) = 5.0575(7) Å) and the diamagnetic nitroprusside anion serves as a terminal entity. This give us an opportunity to study the magnetic exchange of the $Mn^{III}$-$Mn^{III}$ type mediated by water-hydrogen bonds unaffected by bridging through nitroprusside, which is found in the remaining reported complexes. The experimental magnetic data are presented in Fig. 5. The room temperature effective magnetic moment of **6b** is equal to 7.1 $\mu_B$, which is very close to theoretical value of 6.93 $\mu_B$ for two paramagnetic non-interacting centres with $S = 2$ ($g = 2.0$). The susceptibility is increasing on cooling and is reaching its maximum at 6.5 K, which is also accompanied by decrease of $\mu_{eff}$ below 50 K down to 2.1 $\mu_B$ at 1.9 K. The isothermal magnetization at 2 K is not saturated even at $B$ = 7 T and has value of $M_{mol}/N_A\mu_B = 6.2$, which is below the saturation limit of $M_{mol}/N_A\mu_B = 8$ (2 x $S = 2$ and $g = 2.0$). By applying equations 1-3 to both temperature and field dependent magnetic data, we obtained $J = -0.72(1)$ cm$^{-1}$, $g = 2.048(1)$, $D = -3.65(9)$ cm$^{-1}$ and $zj = -0.06(1)$ cm$^{-1}$ (Fig. 5). The negative and large value of $D$-parameter are in agreement with the elongated octahedrons of Mn(III) centres due to the Jahn-Teller effect. However, the chromophores of the respective Mn(III) centres differ in one apical position – $\{MnO_3N_3\}$ for Mn1 and $\{MnO_4N_2\}$ for Mn2 (Fig. 3) and because of that the calculated $D$-value serves as an average value of both distinct Mn(III) centers. The most important outcome is that considerably large magnetic exchange is mediated by hydrogen bonds between Mn(III) centers.

## Trinuclear $[\{Mn(L4)(H_2O)\}_2\{\mu\text{-}Fe(CN)_5NO\}]\cdot x CH_3OH$ complexes 4b and 2b

The compound **4b** shows very similar magnetic properties to compound **6b** (Fig. 5), which justifies the presumption that dominant magnetic exchange is mediated through hydrogen bonds ($d$(Mn···Mn) = 4.7132(9) Å) and not through the diamagnetic nitroprusside anion ($d$(Mn···Mn) = 10.225(2) Å). Thus, the magnetic data of **4b** were treated using the same procedure as for **6b** under the condition that $D_1 = D_2$, because there is only one Mn atom in the asymmetric unit. The resulting parameters are $J = -0.79(1)$ cm$^{-1}$, $g = 1.981(2)$, $D = -3.7(1)$ cm$^{-1}$ and $zj = +0.12(2)$ cm$^{-1}$ (Fig. 5). The last reported Mn(III) compound is complex **2b**, which exhibits comparable properties to compounds **4b** and **6b** (Fig. 5) Thus, we used the same model despite the lack of its X-ray crystal structure. The best fit was obtained with the following parameters: $J = -0.55(1)$ cm$^{-1}$, $g = 1.987(2)$, $D = -3.5(2)$ cm$^{-1}$ and $zj = -0.10(2)$ cm$^{-1}$ (Fig. 5).

## Trinuclear $[\{Fe(L4)(H_2O)\}_2\{\mu\text{-}Fe(CN)_5NO\}]\cdot x CH_3OH$ complexes 2a, 3a, 4a and 5a

The magnetic behaviour of trinuclear Fe(III)-nitroprusside complexes **2a**, **3a**, **4a** and **5a** was found to be very similar (Fig. 6). The room temperature values of the effective magnetic moment are in the range of 8.42–8.57 $\mu_B$, which is very close to theoretical value of 8.37 $\mu_B$ for two paramagnetic non-interacting centres with $S$ = 5/2 ($g$ = 2.0). Upon cooling, the $\mu_{eff}/\mu_B$ dependences are almost constant down to 50 K and then they start to decrease to values of 3.33, 3.46, 2.68 and 2.73 at $T$ = 1.9 K for **2a**, **3a, 4a**, and **5a**, respectively.

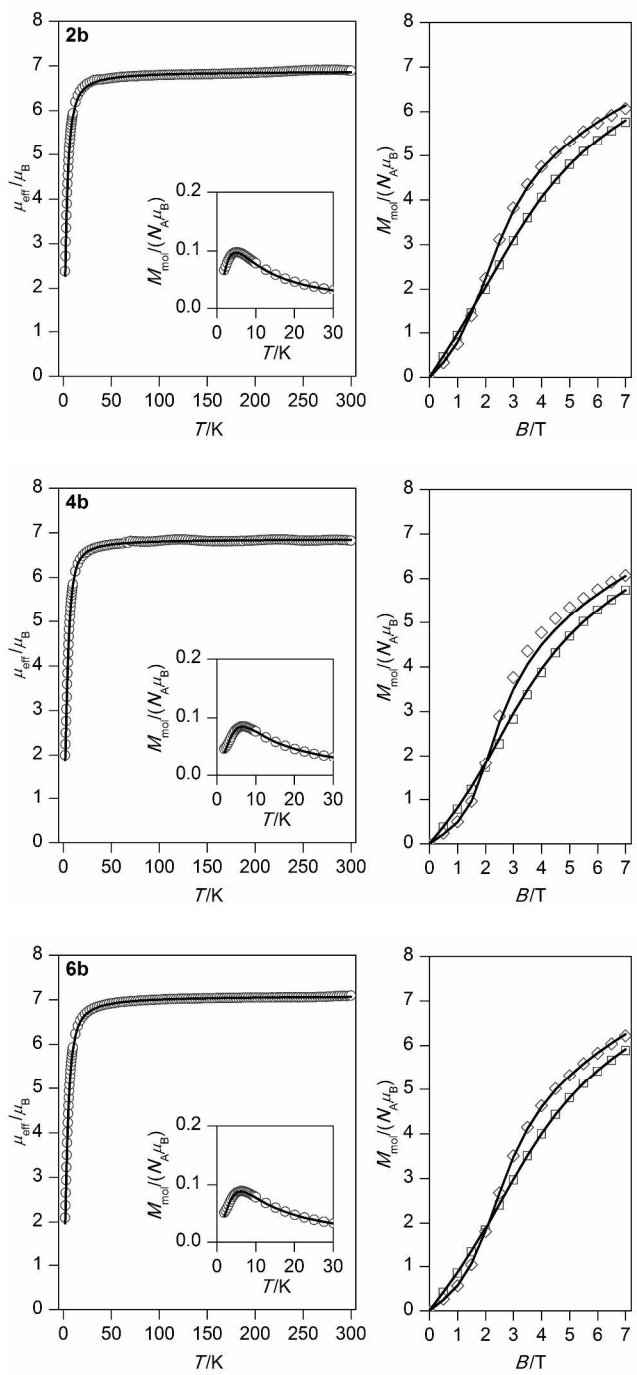


**Fig. 5** Magnetic properties of **2b**, **4b** and **6b**. Each plot shows the temperature dependence of the effective magnetic moment (calculated from the temperature dependence of magnetization at $B = 0.1$ T; inset) and the isothermal magnetizations measured at $T = 2.0$ (◊) and 4.6 K (□). Experimental data – empty symbols, full lines - the best fit calculated with $J = -0.55(1)$ cm$^{-1}$, $g = 1.987(2)$, $D = -3.5(2)$ cm$^{-1}$ and $zj = -0.10(2)$ cm$^{-1}$ for **2b**, $J = -0.79(1)$ cm$^{-1}$, $g = 1.981(2)$, $D = -3.7(1)$ cm$^{-1}$ and $zj = +0.12(2)$ cm$^{-1}$ for **4b** and $J = -0.72(1)$ cm$^{-1}$, $g = 2.048(1)$, $D = -3.65(9)$ cm$^{-1}$ and $zj = -0.06(1)$ cm$^{-1}$ for **6b**.

Also, the maxima of the molar magnetization (or mean molar susceptibility) ranged from 3.5 to 6.5 K. This fact indicates the presence of the antiferromagnetic exchange between Fe(III) mediated by hydrogen bonds and/or also the zero-field splitting of Fe(III) centers. Moreover, the isothermal magnetization measurements at liquid helium temperatures (2.0 and 4.6 K) support this presumption, because the experimental values of $M_{mol}/N_A\mu_B$ are below the theoretical saturation value $M_{mol}/N_A\mu_B = g \cdot S \cdot 2 = 10$ ($g = 2.0$, $S = 5/2$), Fig. 6. Therefore, the same spin Hamiltonian was used as in the equation 1, but in this case $S_1 = S_2 = 5/2$ holds. It must be stressed that including the ZFS term has been essential to responsibly fit all experimental data together. We have found that slightly better fits could be obtained for positive than negative sign of *D*-parameters and both sets are tabulated for each of the presented compound in Table 3 (see also Fig. 6 and Figs. S9-12, ESI). Evidently, the weak antiferromagnetic exchange was found in the range from -0.52 to -1.05 cm$^{-1}$. In the case of *positive D*-parameter, the $|D/J|$ ratios vary between 1.70 and 2.45, but in the case of *negative D*-parameter, the $|D/J|$ ratios vary between 0.50 and 1.15. To summarize, the values of the antiferromagnetic exchange in Mn(III) and Fe(III) compounds **2a-6b** were found to be in narrow interval between –0.52 cm$^{-1}$ and –1.05 cm$^{-1}$, but the ZFS is much larger in case of Mn(III) complexes. This is expected feature for Mn(III) atom due to the Jahn-Teller effect and larger distortion of coordination polyhedral.[33]

Furthermore, we strived to find clear magneto-structural correlation either for isotropic exchange (*J*) or magnetic anisotropy (*D*) in the reported series of compounds taking into account various structural parameters. However, the *D*-parameter does not simply correlate with geometric deformation of coordination chromophore ($\Sigma$), which can be explained by complexity and variedness of donor atoms. Conversely, there are some remarks concerning the isotropic exchange, which must be taken into account: our previous results[20] predicted weaker exchange interactions within the supramolecular dimer $[M(L4)(Solv)]^+\cdots[M(L4)(Solv)]^+$. when Solv = $CH_3OH$ and stronger ones for compounds with Solv = $H_2O$. As can be seen from Table 3 this prediction holds true; the compounds containing $[M(L4)(CH_3OH)]^+$ fragments possess weaker exchange interactions with *J* values ranging from -0.3 to -0.6 cm$^{-1}$ while the $[M(L4)(H_2O)]^+$ compounds have *J* values lower from -0.7 to -1.3 (when not including most probably overestimated *J* values due to the omitting of the ZFS term in the magnetic data analysis, for details see Table 3). From the collected data it seems to be apparent that difference in the quality of the exchange interactions mediation between coordinated methanol and water molecules is not caused by the intrinsic difference found between these two solvents, but it is most probably caused just by the different number of the hydrogen bonds formed by each particular solvent molecule: $CH_3OH$ (2 hydrogen bonds within the dimer), $H_2O$ (usually 4 hydrogen bonds). This can be supported by two examples from the present series of the nitroprusside bridged compounds.

Cite this: DOI: 10.1039/c0xx00000x

www.rsc.org/xxxxxx

# ARTICLE TYPE

**Table 2** Crystallographic data and structure refinement details for the complexes **3a**, **4a**, **4b**, **5** and **6b**

| | **3a**·2CH$_3$OH | **4a** | **4b** | **5a** | **6b**·H$_2$O·CH$_3$OH |
|---|---|---|---|---|---|
| Formula | $C_{47}H_{40}N_{10}O_9Fe_3$ | $C_{45}H_{48}N_{10}O_{11}Fe_3$ | $C_{45}H_{48}N_{10}O_{11}Fe_1Mn_2$ | $C_{47}H_{52}N_{10}O_{11}Fe_3$ | $C_{62.5}H_{50}N_{10}O_{10.5}Fe_1Mn_2$ |
| *Mr* | 1056.44 | 1072.48 | 1070.66 | 1100.54 | 1274.85 |
| *T* / K | 150(2) | 150(2) | 150(2) | 150(2) | 150(2) |
| Crystal system | Triclinic, *P*-1 | Monoclinic, *C*2/*c* | Monoclinic, *P*2$_1$/*c* | Monoclinic, *P*2$_1$/*c* | Triclinic *P*-1 |
| *a* / Å | 10.8773(4) | 23.0051(7) | 13.2000(11) | 13.651(5) | 10.6373(3) |
| *b* / Å | 11.0243(4) | 13.7936(4) | 13.1797(8) | 13.387(5) | 15.3822(4) |
| *c* / Å | 11.6197(4) | 14.7860(4) | 14.860(2) | 15.434(4) | 18.2505(5) |
| $\alpha$ / ° | 99.960(3) | 90.00 | 90.00 | 90.00 | 78.980(2) |
| $\beta$ / ° | 116.960(4) | 96.407(3) | 116.958(8) | 120.29(2) | 79.305(2) |
| $\gamma$ / ° | 105.062(3) | 90.00 | 90.00 | 90.00 | 73.460(2) |
| *V* / Å$^3$ | 1128.77(10) | 4662.6(2) | 2304.3(4) | 2435.5(14) | 2782.45(13) |
| Z | 1 | 4 | 2 | 2 | 2 |
| $D_c$ / g·cm-3 | 1.554 | 1.528 | 1.543 | 1.501 | 1.520 |
| $\mu$ / mm-1 | 1.021 | 0.993 | 0.923 | 0.952 | 0.778 |
| F (0 0 0) | 542 | 2216 | 1104 | 1140 | 1310 |
| Reflections collected/unique | 10554/3948 | 16257/4091 | 18371/4058 | 19415/4240 | 24066/9726 |
| Data/restraints/parameters | 3948/3/320 | 4091/3/322 | 4058/0/315 | 4240/5/364 | 9726/13/815 |
| Goodness-of-fit (GOF) on $F^2$ | 1.110 | 1.043 | 0.875 | 1.052 | 1.009 |
| $R_1$, $wR_2$ ($I > 2\sigma(I)$) | 0.0350/0.0912 | 0.0238/0.0625 | 0.0469/0.0890 | 0.0303/0.0837 | 0.0426/0.0946 |
| $R_1$, $wR_2$ (all data) | 0.0415/0.0928 | 0.0295/0.0638 | 0.0972/0.0965 | 0.0417/0.0861 | 0.0735/0.1000 |

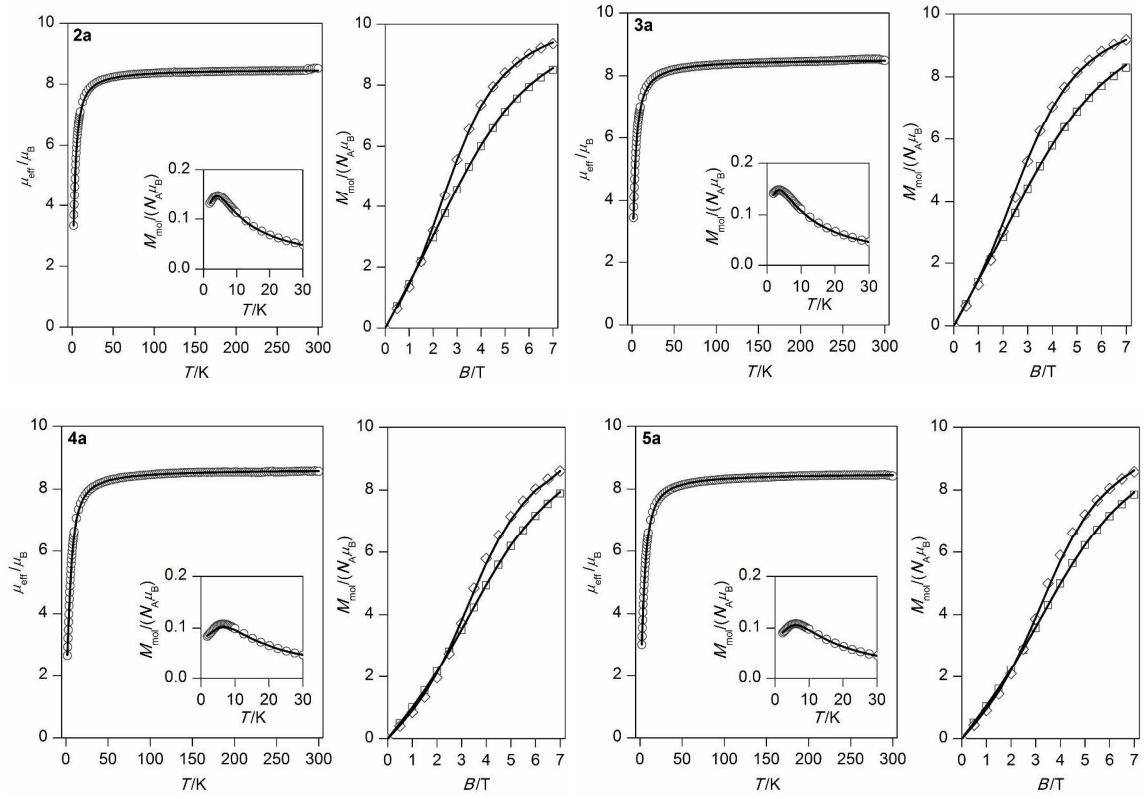


**Fig. 6** Magnetic properties of **2a**, **3**, **4a** and **5a**. Each plot shows the temperature dependence of the effective magnetic moment (calculated from the temperature dependence of magnetization at $B = 0.1$ T; inset) and the isothermal magnetizations measured at $T = 2.0$ (◊) and 4.6 K (□). Experimental data – empty symbols, full lines - the best fit calculated with: $J = -0.64(2)$ cm$^{-1}$, $g = 2.031(2)$, $D = +1.1(2)$ cm$^{-1}$ and $zj = -0.09(2)$ cm$^{-1}$ for **2a**, $J = -0.53(2)$ cm$^{-1}$, $g = 2.042(3)$, $D = +1.3(2)$ cm$^{-1}$ and $zj = -0.24(3)$ cm$^{-1}$ for **3a**, $J = -1.01(4)$ cm$^{-1}$, $g = 2.064(3)$, $D = +1.9(3)$ cm$^{-1}$ and $zj = +0.03(3)$ cm$^{-1}$ for **4a**, $J = -0.94(2)$ cm$^{-1}$, $g = 2.033(1)$, D = +1.6(2) cm$^{-1}$ and $zj = -0.026(4)$ cm$^{-1}$ for **5a**.

Cite this: DOI: 10.1039/c0xx00000x

www.rsc.org/xxxxxx

# ARTICLE TYPE

The compound **3a** represents a novel structural type of the $[M(L4)(H_2O)]^+\cdots[M(L4)(H_2O)]^+$ supramolecular dimer which is held by two hydrogen bonds whereas two other remaining hydrogen atoms point to the lattice solvent molecules (Fig. 2, Fig. 7). Noticeably, the value of the coupling constant ($J$ = –0.52 cm$^{-1}$) is very similar to those observed for the compounds with Solv = $CH_3OH$ (Table 3). Furthermore, the compound **6b** has another unique asymetric dimeric synthon with three supportive hydrogen bonds (Fig. 3, Fig. 7). The strength of the exchange interaction is in between the values typical for $CH_3OH$ and $H_2O$ with $J$ = 0.72 cm$^{-1}$.

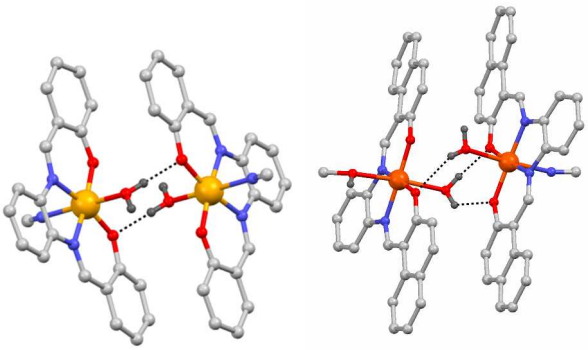

**Fig. 7** A detailed view on novel types of the "supramolecular dimers" in **3a** (left) and **6b** (right). The hydrogen atoms are omitted for clarity, except for the atoms involved in hydrogen bonding (black dashed lines).

## DFT calculations

In order to support our conclusions from magnetochemical analyses of the experimental data, we performed the isotropic exchange parameters' calculations using the DFT method for H-bond bridged dinuclear molecular fragments $[\{M^{III}(L4)(H_2O)(NC)\}_2]$ (M = Fe, Mn) for compounds reported here **3a–6b**, and also for similar compounds reported in literature, **7a-7e.** Moreover, we investigated also the role of the diamagnetic nitroprusside anion in mediation of magnetic exchange for compound **4a** using the $[\{Fe^{III}(L4c)(H_2O)\}_2\{\mu\text{-}Fe^{II}(CN)_5NO\}]$ molecular fragment.

All the calculations were based on experimental X-ray geometries except for **7a**, where some hydrogen atoms were missing in CSD deposited data (CCDC IGAKEG), and their atomic positions were optimized with the BP86 functional and def2-TZVP(-f) basis set.

As this work extend our research of magnetic exchange in transition metal complexes containing diamagnetic bridging polythiocyanidoplatinate,[20,21] the same hybrid functional B3LYP together with def2-TZVP basis set and the scalar relativistic second-order Douglas–Kroll–Hess Hamiltonian were used.

Therefore, the results of relevant hydrogen bonds bridged compounds, $[\{Mn(L4o)(H_2O)\}_2\{\mu\text{-}Pt(SCN)_6\}]$ (**8**) and $[\{Mn(L4n)(H_2O)\}_2\{\mu\text{-}Pt(SCN)_4\}]$ (**9**), $[\{Mn(L4b)(CH_3OH)\}_2\{\mu\text{-}Pt(SCN)_4\}]$ (**10**), $[\{Mn(L4p)(CH_3OH)\}_2\{\mu\text{-}Pt(SCN)_4\}]$ (**11**), where $L4n^{2-}$ = *N,N′*-benzene-bis(4-aminodiethylenesalicylideneiminate) dianion, $L4o^{2-}$ = *N,N′*-3-methylbenzene-bis(3-ethoxysalicylideneiminate) dianion, $L4p^{2-}$ = *N,N′*-ethylene-bis(naphthylidenebenzeneiminate) dianion, were also included in Table 3.

The isotropic exchange analysis was based on the following Heisenberg spin Hamiltonian

$$\hat{H} = -J\left(\vec{S}_1 \cdot \vec{S}_2\right) \quad (4)$$

and evaluation of energy difference between high-spin (HS) and broken-symmetry (BS) spin states, $\Delta = E_{BS} - E_{HS}$, using quantum-chemical computational software ORCA. The final $J$-values were calculated by the Ruiz's

$$J^{Ruiz} = \Delta / \left(2S_1S_2 + S_1\right) \quad (5)$$

and Yamaguchi's

$$J^{Yam} = 2\Delta / \left(\left\langle S^2\right\rangle_{HS} - \left\langle S^2\right\rangle_{BS}\right) \quad (6)$$

approaches and are tabulated for $[\{M^{III}(L_i)(H_2O)(NC)\}_2]$ fragments in Table 3. HS spin states had small spin contamination, which is manifested by the calculated $\langle S^2\rangle_{HS}$ values that are close to the theoretical values $\langle S^2\rangle_{HS} = S(S+1)$ where $S$ = 5 for M = Fe and $S$ = 4 for M = Mn ($S_{HS}$ is the total spin value for the HS state), while BS spin states's $\langle S^2\rangle_{LS}$ values are close to $M_S^2 + S_{HS}$ ($M_S$ is spin projection of the BS spin state).

First, the DFT calculation for $[\{Fe^{III}(L_3)(H_2O)\}_2\{\mu\text{-}Fe^{II}(CN)_5NO\}]$ molecular fragment of **4a** resulted in trifling magnetic exchange, $J^{Yam}$ = +0.031 cm$^{-1}$ ($J^{Ruiz}$ = +0.026 cm$^{-1}$), thus supporting our presumption that this superexchange path is very inefficient in promoting magnetic exchange.

Next, the calculation performed for H-bonded dimers $[\{M^{III}(L4)(H_2O)(NC)\}_2]$ (M = Fe, Mn) resulted in the $J$-values tabulated in Table 3. The $J^{Yam}$-values were found in the range from –0.54 to –0.60 cm$^{-1}$ for $[\{Fe^{III}(L4)(H_2O)(NC)\}_2]$ (**3a**, **4a** and **5a**), and in the range from –0.56 to –0.94 cm$^{-1}$ for $[\{Mn^{III}(L4)(H_2O)(NC)\}_2]$ and $[\{Mn^{III}(L4)(H_2O)(NCS)\}_2]$ (**2b-6b** and **7b-11**). The good congruence between $J$-values derived from magnetochemical analysis of the experimental data and DFT calculations was obtained for compounds **3a**, **4b**, **6b** and **7b**, when taking into account the $J^{Yam}$ values. However, the larger discrepancies were observed for the remaining compounds, e.g. in case of **4a** magnetic analyses resulted in $J_{mag} \approx -1.0$ cm$^{-1}$, which is in contrast to the values of $J^{Ruiz}$ = –0.48 cm$^{-1}$ or $J^{Yam}$ = –0.57 cm$^{-1}$ (Table 3). The question then arises: why the same used DFT method resulted in so unequal results in comparison to magnetic analysis? We can speculate that these discrepancies are due to small changes in the crystal structures, which may occur at lower temperature than that used for X-ray analysis. To testify this possibility, we performed constrained geometry optimization for $[\{Fe^{III}(L4c)(H_2O)(NC)\}_2]$ molecular fragment of **4a**, where the Fe···Fe distance was varied between 4.4 and 4.9 Å. The geometry was optimized using the BP86 functional with def2-TZVP(-f) basis set together with conductor-like screening model (COSMO), van der Waals corrections (VDW10) and the relativistic effects with the scalar relativistic second-order

Douglas–Kroll–Hess Hamiltonian (DKH2). Afterwards, the *J*-values were calculated at the B3LYP+DKH2/def2-TZVP level of theory for each of the optimized molecular structures to ensure the same condition as that used for molecular fragments of **3a-11** based on their X-ray structures.

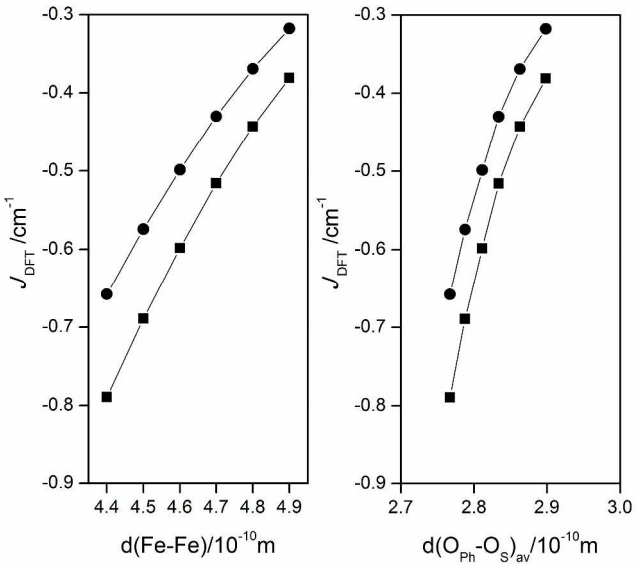


**Fig. 8** The calculated isotropic exchange $J^{Ruiz}$ (circles) and $J^{Yam}$ (squares) as a function of the Fe···Fe distance (left) and the $O_{Ph}$···$O_S$ (right) in the molecular fragment [{Fe(L4c)($H_2O$)(NC)}$_2$] of **4a** calculated using B3LYP+DKH2/def2-TZVP, while the molecular geometries were optimized using BP86+COSMO+VDW10+DKH2/def2-TZVP(-f).

This resulted in magneto-structural correlation depicted in Fig. 8 from which we can conclude that the antiferromagnetic exchange is increasing with decreasing the Fe···Fe separation. However, the approximate change of $\Delta(J_{DFT})/\Delta(d_{Fe\text{-}Fe}) \approx 0.5–1.0$ cm$^{-1}$/Å cannot explain itself large discrepancies between $J_{DFT}$ and $J_{mag}$ in the case of possibly small changes in crystal structure induced by cooling to very low temperature.

Thus, we also tested another hypothesis related to positions of hydrogen atoms in molecular/crystal structure. It is well known that the determination of the hydrogen atom positions from the X-ray analysis can be potentially inaccurate, especially when the hydrogen atoms are bonded to atoms with high electronegativity such as oxygen or nitrogen atoms. This was pointed out also in several DFT studies devoted to problematic of magnetic exchange mediated by hydrogen bonds in other transition metal complexes.[29] Due to these reasons we have to strive out how the position of hydrogen atoms influences the magnetic exchange interactions. Therefore, the positions of hydrogen atoms involved in magnetic exchange pathway (in H-bond bridged dinuclear molecular fragments [{$M^{III}$(L4)($H_2O$)(NC)}$_2$] (M = Fe, Mn) (**4a**, **5a**, **4b**, **7a**, and **7e**) and also for [{Mn(L4)($H_2O$)(NCS)}$_2$] (**8** and **9**), while keeping all other atoms in the same positions as determined from their X-ray structures) were optimized using the BP86/def-TZVP(-f). The situation for other complexes, namely **3a**, **6b**, **7b** and **7d** is more complex, because water molecules are not only involved in hydrogen bonds between closest metal atoms, but also form hydrogen bonds to methanol molecules (**3a** and **7b**) or to cyanido ligands of the nitroprusside anions from other supramolecular chains (**6b** and **7d**), so they were excluded.

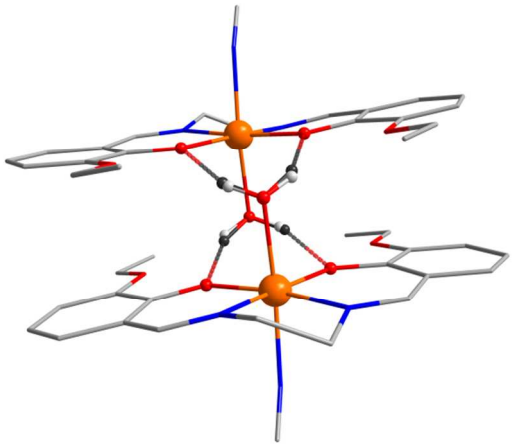

**Fig. 9** Molecular fragment [{Fe(L4c)($H_2O$)(NC)}$_2$] of **4a**: the comparison of hydrogen atom positions based on X-ray structure (light gray balls) and based on geometry optimized using BP86/def2-TZVP(-f) (dark gray balls). The rest of hydrogen atoms not involved into the formation of supramolecular dimer were omitted for clarity.

The H-atoms geometry optimization procedure for molecular fragments **4a**, **5a**, **4b**, **7a**, **7e** and **8-11** generally resulted in the increase of the O–H bonds, which can be demonstrated for O–H distances of water molecules in **4a**: $d(O–H)_{X\text{-}ray}$ = 0.831 and 0.837 Å and $d(O–H)_{DFT}$ = 0.989 and 0.994 Å (Fig. 9). In next step, the *J*-values were calculated using B3LYP+DKH2/def2-TZVP and resulted in much larger antiferromagnetic exchange constants (Table 3), which can be exemplified again for **4a**: $J^{Ruiz}$ = –0.81 cm$^{-1}$ or $J^{Yam}$ = –0.98 cm$^{-1}$ and especially the latter value is almost identical to $J_{mag} \approx –1.0$ cm$^{-1}$ determined from magnetic analysis.

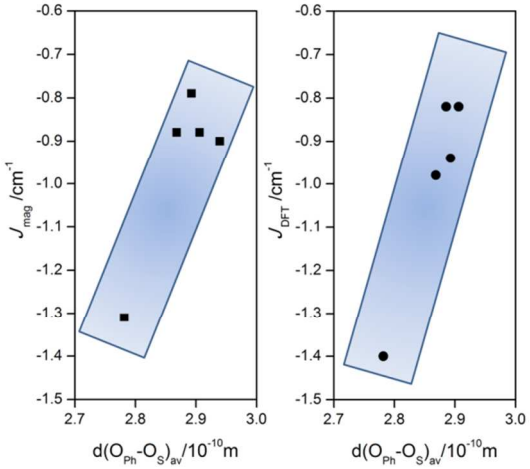


**Fig. 10** The isotropic exchange J-values as a function of the average $O_{Ph}$···$O_S$ distance in Mn(III) compounds molecular compounds **4b**, **7a**, **7e**, **8** and **9**, either derived from magnetic analysis (left) or calculated by DFT using B3LYP+DKH2/def2-TZVP on geometries in which only the hydrogen atoms were optimized using BP86/def2-TZVP(-f).

These results demonstrate much larger sensitivity of magnetic exchange to position of hydrogen atom within the O–H···O hydrogen bond than to the M···M distance, which can explain some discrepancies observed between *J*-values derived from magnetic analysis and DFT calculations based on X-ray molecular structures. Furthermore, there is a clear evidence that

*J*-value correlates with averaged $O_{Ph}\cdots O_S$ distance both in Fe(III) and Mn(III) complexes as demonstrated in Figure 8 and Figure 10, respectively.

**Table 3** Summary of structural details, results from magnetic analysis and DFT calculations for iron(III) and manganese(III) nitroprusside/polythiocyanidoplatinate-bridged complexes.

| | Selected structural data[a] | | | | Magnetic analysis data[b] | | | | DFT calculated data | |
|---|---|---|---|---|---|---|---|---|---|---|
| Compound | M···M* (Å) | M···M (Å) | $O_{Ph}\cdots O_{Ph}$* (Å) | $O_{Ph}\cdots O_S$* (Å) | *J* ($cm^{-1}$) | *g* | *D* ($cm^{-1}$) | *zj* ($cm^{-1}$) | $\langle S^2\rangle_{HS}/\langle S^2\rangle_{BS}$ | $J^{Ruiz}/J^{Yam}$ ($cm^{-1}$) |
| **2a** | – | – | – | – | −0.64(2)<br>−0.67(5) | 2.031(2)<br>2.033(3) | +1.1(2)<br>−0.48(7) | –0.09(2)<br>–0.13(5) | | |
| **3a** | 4.8728(5) | 10.1621(6) | 3.682(2) | 3.459(2)<br>2.690(3) | −0.53(2)<br>−0.52(6) | 2.042(3)<br>2.044(3) | +1.3(2)<br>−0.6(1) | –0.24(3)<br>–0.29(5) | 30.02/5.02<br>30.02/5.02 | –0.45/–0.54 |
| **4a** | 4.5608(4) | 10.1532(5) | 3.263(2) | 2.927(2)<br>2.792(2) | −1.01(4)<br>−1.00(5) | 2.064(3)<br>2.070(3) | +1.9(3)<br>–0.69(7) | +0.03(3)<br>–0.12(6) | 30.02/5.02<br>30.02/5.02 | –0.48/–0.57<br>–0.81/–0.98[f] |
| **5a** | 4.593(2) | 10.173(4) | 3.338(2) | 2.865(2)<br>2.814(2) | −0.94(2)<br>−1.05(4) | 2.033(1)<br>2.036(2) | +1.6(2)<br>–0.53(5) | –0.026(4)<br>–0.02(4) | 30.02/5.02<br>30.02/5.02 | –0.50/–0.60<br>–0.86/–1.04[f] |
| **2b** | | | | s | −0.55(1) | 1.987(2) | −3.5(2) | –0.10(2) | | |
| **4b** | 4.7132(9) | 10.225(2) | 3.296(3) | 2.934(3)<br>2.851(3) | −0.79(1) | 1.981(2) | −3.7(1) | +0.12(2) | 20.07/4.07<br>20.07/4.07 | –0.59/–0.74<br>–0.94/–1.16[f] |
| **6b** | 5.0575(7) | – | 3.534(3)<br>3.579(3) | 3.243(3)<br>3.022(3) | −0.72(1) | 2.048(1) | −3.65(9) | –0.06(1) | 20.07/4.07 | –0.55/–0.68 |
| **7a** | 4.690(2) | 10.358(3) | 3.339(5) | 2.907(6)<br>2.830(7) | –0.88[c] | 2.05 | –2.62 | – | 20.06/4.06 | –0.98/–1.24[f] |
| **7b** | 5.152(3) | 10.288(3) | 3.803(5) | 3.338(4)<br>2.790(6) | –0.90[d] | 2.02 | –2.46 | – | 20.07/4.07 | –0.71/–0.89 |
| **7d** | 5.067(2) | 10.400(2) | 3.496(6)<br>3.748(6) | 3.089(6)<br>2.910(6) | –1.90[e] | 2.0 | – | – | 20.08/4.08 | –0.61/–0.76 |
| **7e** | 4.694(1) | 10.388(3) | 3.303(2) | 2.913(2)<br>2.858(2) | – | – | – | – | 20.07/4.07<br>20.07/4.07 | –0.50/–0.62<br>–0.82/–1.04[f] |
| **8** | 4.7007(9) | 12.5840(8) | 3.242(4) | 2.882(4)<br>2.930(5) | –0.88 | 2.09 | -3.06 | +0.21 | 20.09/4.09<br>20.08/4.08 | –0.45/–0.56<br>–0.82/–1.02[f] |
| **9** | 4.858(2) | 12.017(2) | 3.365(8)<br>3.550(8) | 2.707(8),<br>2.806(8)<br>2.779(8),<br>2.834(8) | –1.31(6) | 1.848(2) | –2.2(1) | –0.41(5) | 20.07/4.07<br>20.07/4.07 | –0.76/–0.94<br>–1.40/–1.74[f] |
| **10** | 5.004(2) | 12.044(2) | 3.469(3) | 2.728(3) | -0.53(1) | 1.879(2) | -4.6(2) | +0.23(2) | 20.08/4.08 | –0.54/–0.68 |
| **11** | 5.0682(2) | 11.749(3) | 3.764(2) | 2.777(2) | -0.47(1) | 1.889(2) | -3.6(1) | +0.03(1) | 20.08/4.08 | –0.33/–0.42 |

[a] M···M* is shortest distance between metal atoms bridged through water mediated hydrogen bonds; M···M is shortest distance between metal atoms bridged by nitroprusside or polythiocyanidoplatinate; $O_{Ph}\cdots O_{Ph}$* and $O_{Ph}\cdots O_S$* are distances between oxygen atoms of phenol groups or phenol group and oxygen atom of water/methanol molecule attached to different metal atoms M and M*. [b] *J*-values reported in literature were scaled according to spin Hamiltonian in equation 1. [c] ref 22., [d] ref 23.[e] ref 24, comment*:* *J*-value is most probably overestimated due to omitting ZFS term. [f] results based on DFT calculations performed on molecular fragments, in which hydrogen atoms were optimized with BP86/def2-TZVP(-f).

## Experimental Section

### Materials.

All the starting chemicals were of analytical reagent grade and were used as received. $FeCl_3\cdot 6H_2O$, $MnCl_2\cdot 4H_2O$, $Na_2[Fe(CN)_5NO]\cdot 2H_2O$ and solvents were obtained from the commercial sources and the organic compounds 1,2-diaminocyclohexane, 1,2-diamino-benzene, ethane-1,2-diamine, propane-1,2-diamine, 2-hydroxy-benzaldehyde, 4-hydroxy-1-naphthaldehyde, 3-ethoxy-2-hydroxybenzaldehyde and triethylamine ($Et_3N$), (Sigma-Aldrich Co., Acros Organics Co., Lachema Co. and Fluka Co.).

### Synthesis of the tetradentate Schiff base $H_2$L4a- $H_2$L4e

These organic compounds where prepared by the Schiff base condensation between the following derivatives, i.e. 2-hydroxybenzaldehyde ($H_2$L4a or $H_2$L4c), 4-hydroxy-1-naphthaldehyde ($H_2$L4e) or 3-ethoxy-2-hydroxybenzaldehyde ($H_2$L4b or $H_2$L4d) and the corresponding diamines, i.e. 1,2-diaminocyclohexane ($H_2$L4a), 1,2-diaminobenzene ($H_2$L4b or $H_2$L4e), ethane-1,2-diamine ($H_2$L4c) or propane-1,2-diamine ($H_2$L4d). Reaction mixture of 20 mL of methanol solutions of respective derivatives of benzaldehyde (5 mmol) and diamine (2.5 mmol) in 10 mL of methanol was stirred under reflux at 40 °C for 2 hours, and it resulted in yellow powder material after the solvent evaporation. The solid powdered substance was washed with diethyl ether and dried in a vacuum; yield was higher than 97 %.

### Synthesis of the precursors [Fe(L4a)Cl] (1a) [Mn(L4a)Cl] (1b), [Fe(L4b)Cl] (1c), [Fe(L4c)Cl] (1d), [Mn(L4c)Cl] (1e), [Fe(L4d)Cl] (1f) and [Mn(L4e)Cl] (1g)

The solution of 10 mmol of $FeCl_3\cdot 6H_2O$ or $MnCl_2\cdot 4H_2O$ in 10 mL of methanol was added to a solution of 10 mmol of $H_2$L4a-$H_2$L4e in 20mL of ethanol. The mixture was stirred for 10 min, and then 20mmol of triethylamine in ethanol (10 mL) was added. The resulting solution was refluxed for 2 h, then after cooling diethyl ether was added which resulted in precipitation of black or brown powder. The solid was filtered off, washed with diethyl ether and dried in a vacuum yield was higher than 90 %.

### Synthesis of the complexes 2a-6b

The dark-brown crystals or dark powder of complexes **2a-6b**

have been obtained from a methanol solution (40 mL) of the complexes **1a-1g** (0.2 mmol) combined with a methanol/water mixture (1:1) of $Na_2[Fe(CN)_5NO]\cdot 2H_2O$ (0.1 mmol). The solution was stirred at room temperature for 4 h. slow evaporation of the resulting solution at room temperature afforded black single crystals suitable for X-ray diffraction of the complexes after a week. Black crystals were filtered off, washed twice with water, diethyl ether and dried in a vacuum.

**[{Fe(L4a)(H$_2$O)}$_2${$\mu$-Fe(CN)$_5$(NO)}]·CH$_3$OH (2a)**. Yield: 76%, Anal. Calcd. for $C_{46}H_{48}N_{10}O_8Fe_3$: C, 53.30; H, 4.66; N, 13.51. Found: C, 53.52; H, 4.53; N, 13.70%. $\Lambda_M$ (DMF, $S\cdot cm^2\cdot mol^{-1}$): 5.2. FT-IR (Nujol, $cm^{-1}$): 517m; 486m; 474m; 444m; 431w; 369s; 342m; 329m; 296m ν(Fe−N); 275w; 245w ν(Fe−O); 236m; 185w; 174w. FT-IR (KBr, $cm^{-1}$): 3115w; 3037w $\nu(C-H)_{ar}$; 2872w; 2987w $\nu(C-H)_{alip}$; 2939w $\nu(C-H)_{alip}$; 2152m ν(C≡N); 1917m ν(N=O); 1625vs $\nu(C=N)_{ar}$; 1595m; 1541m; 1472m $\nu(C=C)_{ar}$; 1452vs $\nu(C=C)_{ar}$; 1357w; 1274w; 1222w; 1193w; 1157w; 1114w; 1110w; 1039w; 1018w; 945w; 858w; 752m.

**[{Mn(L4a)(H$_2$O)}$_2${$\mu$-Fe(CN)$_5$(NO)}]·CH$_3$OH (2b)**. Yield: 75%, Anal. Calcd. for $C_{46}H_{48}N_{10}O_8Mn_2Fe_1$: C, 53.39; H, 4.67; N, 13.53. Found: C, 53.54; H, 4.57; N, 13.74%. $\Lambda_M$ (DMF, $S\cdot cm^2\cdot mol^{-1}$): 11.5. FT-IR (Nujol, $cm^{-1}$): 572w; 539w; 510w; 468m; 455w; 438w; 419w; 379m; 333w; 322w; 286m ν(Mn−N); 259w ν(Mn−O); 209w. FT-IR (KBr, $cm^{-1}$): 3132w; 3021w $\nu(C-H)_{ar}$; 2931w $\nu(C-H)_{alip}$; 2859w; 2163m ν(C≡N); 1922m ν(N=O); 1618vs $\nu(C=N)_{ar}$; 1596m; 1544m; 1468m $\nu(C=C)_{ar}$; 1443m $\nu(C=C)_{ar}$; 1395w; 1307w; 1286w; 1268w; 1233w; 1196w; 1148w; 1052w; 1006w; 995w; 907w; 851w; 753m; 677w.

**[{Fe(L4b)(H$_2$O)}$_2${$\mu$-Fe(CN)$_5$(NO)}]·2CH$_3$OH (3a)**. Yield: 71%, Anal. Calcd. for $C_{47}H_{40}N_{10}O_9Fe_3$: C, 53.43; H, 3.81; N, 13.25. Found: C, 53.56; H, 3.52; N, 13.71%. $\Lambda_M$ (DMF, $S\cdot cm^2\cdot mol^{-1}$): 15.2. FT-IR (Nujol, $cm^{-1}$): 568w; 554w; 515w; 491w; 460m; 426w; 390w; 352m; 332w; 306w; 285m ν(Fe−N); 267w; 241m ν(Fe−O); 217w; 198w. FT-IR (KBr, $cm^{-1}$): 3372w; 3299w; 3217w; 3118w; 3025w $\nu(C-H)_{ar}$; 2932w $\nu(C-H)_{alip}$; 2139m ν(C≡N); 1906m ν(N=O); 1613vs $\nu(C=N)_{ar}$; 1539m; 1467m $\nu(C=C)_{ar}$; 1446m $\nu(C=C)_{ar}$; 1398w; 1314m; 1268w; 1230w; 1023w; 997w; 904w; 809w; 753m; 661w.

**[{Fe(L4c)(H$_2$O)}$_2${$\mu$-Fe(CN)$_5$(NO)}] (4a)**. Yield: 72% Anal. Calcd. for $C_{45}H_{48}N_{10}O_{11}Fe_3$: C, 50.39; H, 4.51; N, 13.06. Found: C, 50.52; H, 4.69; N, 13.33%. $\Lambda_M$ (DMF, $S\cdot cm^2\cdot mol^{-1}$): 21.8. FT-IR (Nujol, $cm^{-1}$): 508m; 492m; 475m; 446w; 437w; 372vs; 344m; 318m; 288w ν(Fe−N); 248m ν(Fe−O); 224w; 170w. FT-IR (KBr, $cm^{-1}$): 3445w; 3414w; 3047w $\nu(C-H)_{ar}$; 2992w $\nu(C-H)_{alip}$; 2942w $\nu(C-H)_{alip}$; 2882w; 2141m ν(C≡N); 1882vs ν(N=O); 1616vs ν(C=N); 1581m; 1552m; 1468m $\nu(C=C)_{ar}$; 1437m $\nu(C=C)_{ar}$; 1395w; 1347w; 1295m; 1250m; 1211w; 1174w; 1141w; 1112w; 1074m; 1055w; 1021w; 947w; 857w; 841w; 774w; 732w; 692w.

**[{Mn(L4c)(H$_2$O)}$_2${$\mu$-Fe(CN)$_5$(NO)}] (4b)**. Yield: 65% Anal. Calcd. for $C_{45}H_{48}N_{10}O_{11}Mn_2Fe_1$: C, 50.48; H, 4.51; N, 13.08. Found: C, 50.55; H, 4.64; N, 13.27%. $\Lambda_M$ (DMF, $S\cdot cm^2\cdot mol^{-1}$): 16.5. FT-IR (Nujol, $cm^{-1}$): 515m; 491m; 469m; 452m; 429w; 378s; 351m; 311m ν(Mn−N); 254w ν(Mn−O); 239m; 170w. FT-IR (KBr, $cm^{-1}$): 3443w; 3412w; 3072w $\nu(C-H)_{ar}$; 3056w $\nu(C-H)_{ar}$; 2996w $\nu(C-H)_{alip}$; 2926w $\nu(C-H)_{alip}$; 2877w; 2138m ν(C≡N); 1874vs ν(N=O); 1614vs ν(C=N); 1579m; 1550m; 1465m $\nu(C=C)_{ar}$; 1438m $\nu(C=C)_{ar}$; 1393w; 1346w; 1298m; 1254m; 1216w; 1178w; 1153w; 1108w; 1083m; 1050w; 1018w; 953w; 894w; 843w; 779w; 763w; 732m; 690w; 603m.

**[{Fe(L4d)(H$_2$O)}$_2${$\mu$-Fe(CN)$_5$(NO)}] (5a)**. Yield: 70% Anal. Calcd. for $C_{47}H_{52}N_{10}O_{11}Fe_3$: C, 51.29; H, 4.76; N, 12.72. Found: C, 50.91; H, 4.55; N, 12.54%. $\Lambda_M$ (DMF, $S\cdot cm^2\cdot mol^{-1}$): 14.2. FT-IR (Nujol, $cm^{-1}$): 518m; 489m; 452m; 449m; 431w; 354s; 303m; 284m ν(Fe−N); 276w; 246w ν(Fe−O); 241m. FT-IR (KBr, $cm^{-1}$): 3348w; 3268w; 3061w $\nu(C-H)_{ar}$; 2981w $\nu(C-H)_{alip}$; 2930w $\nu(C-H)_{alip}$; 2880w; 2149s ν(C≡N); 1882vs ν(N=O); 1616vs ν(C=N); 1594s; 1552m; 1463m $\nu(C=C)_{ar}$; 1443vs $\nu(C=C)_{ar}$; 1391m; 1345w; 1322w; 1295m; 1250m; 1218m; 1180w; 1110w; 1076w; 1037w; 1014w; 895w; 850w; 762w; 731m; 605w.

**[{Mn(L4e)(H$_2$O)(CH$_3$OH)][{Mn(L4e)(H$_2$O)}{$\mu$-Fe(CN)$_5$(NO)}]·H$_2$O·CH$_3$OH (6b)**. Yield: 63% Anal. Calcd. for $C_{63}H_{49}N_{10}O_{10}Mn_2Fe_1$: C, 59.44; H, 3.95; N, 11.00. Found: C, 59.58; H, 3.66; N, 11.27%. $\Lambda_M$ (DMF, $S\cdot cm^2\cdot mol^{-1}$): 91.2. FT-IR (Nujol, $cm^{-1}$): 525m; 492m; 453m; 447m; 434w; 355s; 351m; 305m 278m ν(Mn−N); 248w; 233m ν(Mn−O); 213w. FT-IR (KBr, $cm^{-1}$): 3457m; 3398w; 3074w $\nu(C-H)_{ar}$; 2987w $\nu(C-H)_{alip}$; 2978w $\nu(C-H)_{alip}$; 2875w; 2152s ν(C≡N); 1886vs ν(N=O); 1614vs ν(C=N); 1587s; 1549m; 1474m $\nu(C=C)_{ar}$; 1454vs $\nu(C=C)_{ar}$; 1387m; 1332w; 1319w; 1287m; 1245m; 1217m; 1184w; 1122w; 1097w; 1017w; 889w; 867w; 787w; 745m; 645w.

### General methods

Elemental analysis (CHNS) was performed on an FLASH 2000 CHNS Analyzer (ThermoFisher Scientific). Infrared spectra of the complexes were recorded on a ThermoNicolet NEXUS 670 FT-IR spectrometer using the KBr technique on the diamond plate in the range of 400–4000 $cm^{-1}$ and Nujol techniques in the range of 150–600 $cm^{-1}$. Thermogravimetric (TG) and differential thermal analyses (DTA) were measured on an Exstar TG/DTA 6200 thermal analyzer (Seiko Instruments Inc.). TG/DTA studies were performed in ceramic pans from laboratory temperature to 850 °C with a 2.5 °C $min^{-1}$ temperature gradient in dynamic air atmosphere (100 mL $min^{-1}$).

### Single-crystal X-ray analysis details

X-ray measurements on the selected crystals of **3a-6b** were performed on an Oxford Diffraction Xcalibur$^{TM2}$ equipped with a Sapphire2 CCD detector using the Mo-Kα radiation at 100 K. The CrysAlis program package (version 1.171.33.52, Oxford Diffraction) was used for data collection and reduction.[34] The molecular structures were solved by direct methods SHELX-97 and all non-hydrogen atoms were refined anisotropically on $F^2$ using full-matrix least-squares procedure SHELXS-97[35]. All the hydrogen atoms were found in differential Fourier maps and their parameters were refined using a riding model with $U_{iso}(H) = 1.2$ (CH, $CH_2$, OH) or $1.5U_{eq}$ ($CH_3$). Non-routine aspects of the structure refinement are as follows: in the compounds **3a**, **4a**, **5a** and **6b** the Fe atom of nitroprusside lies at the inversion center with disorder of the nitrosyl and cyanido groups in two *trans* positions. Occupation factors for both disordered parts were set to 0.5.

### DFT calculations

The theoretical calculations were done with the ORCA 2.9.1 computational package. The magnetic exchange (*J*) was

calculated using the hybrid B3LYP functional.[36] The broken-symmetry (BS) spin state was generated by "Flip-Spin" feature of the ORCA program and the isotropic exchange constants *J* were calculated both by the Ruiz's formula[37] and Yamaguchi approach.[38] The polarized triple-ζ quality basis set (def2-TZVP) proposed by Ahlrichs and co-workers has been used for all atoms.[39] The relativistic effects were dealt with the scalar relativistic second-order Douglas-Kroll-Hess Hamiltonian (DKH2) together with relativistically recontracted version of the def2-TZVP basis set.[40] The calculations utilized the RI approximation with the decontracted auxiliary def2-TZVP/J Coulomb fitting basis set and the chain-of-spheres (RIJCOSX) approximation to exact exchange[41] as implemented in ORCA. Increased integration grids (Grid5 and Gridx5 in ORCA convention) and tight SCF convergence criteria were used in all calculations. The geometry optimization of molecular fragment $[\{Fe(L_3)(H_2O)(NC)\}_2]$ (**4a**) were done using the BP86 functional[42] with the def2-TZVP(-f) basis set together with conductor-like screening model (COSMO),[43] van der Waals corrections (VDW10)[44] and DKH2. The positions of hydrogen atoms in H-bond bridged dinuclear molecular fragments $[\{M^{III}(L4)(H_2O)(NC)\}_2]$ (M = Fe, Mn) (**4a**, **5a**, **4b**, **7a**, and **7e**) and also for $[\{Mn(L4)(H_2O)(NCS)\}_2]$ (**8** and **9**) were performed again with BP86/de2-TZVP(-f).

## Conclusions

We have reported the synthesis of trinuclear iron(III) and manganese(III) (**2a-5a**) and dinuclear manganese(III) (**6b**) Schiff base complexes utilizing the nitroprusside anion, $[Fe^{II}(CN)_5NO]^{2-}$, as a building block. The compounds were characterized by various physical methods (elemental analysis, FT-IR, TG/DTA, single-crystal X-ray analysis), which clearly confirmed their compositions and molecular/crystal structures. It was observed that coordinated water molecules are responsible for formation of supramolecular 1D chains (**3a-5a**) or supramolecular dimers (**6b**) through hydrogen bonds of the type O–H···O. The thorough magnetic analysis, which consisted in the concurrent fitting of temperature and field dependent powder magnetic data, played an important role in proper identifying values of the isotropic exchange *J*-parameters and zero-field splitting *D*-parameters.

This enabled us in harmony with DFT calculations of *J*-parameters to confirm weak antiferromagnetic exchange ($J \approx -0.5$ to $-1.3$ $cm^{-1}$) between metal atoms mediated by O–H···O hydrogen bonds, while super-exchange path through diamagnetic the nitroprusside anion was found negligible. Moreover, the detailed DFT study was performed to explain some discrepancies between *J*-values derived from magnetic analysis and DFT calculations themselves. We demonstrated that such DFT calculations are very susceptible to position of hydrogen atoms within the O–H···O hydrogen bond forming super-exchange pathway. To summarize, the strength of magnetic exchange in this class of complexes is controlled by number of $O_S$–H···$O_{Ph}$ hydrogen bonds between metal atoms and by $O_S$···$O_{Ph}$ distance between phenolic oxygen of salen-type ligand ($O_{Ph}$) and oxygen of solvent (water, methanol) coordinated to next metal atom ($O_S$). These results help to understand magnetic exchange interactions through hydrogen bonding within the supramolecular $[M^{III}(L4)(Solv)]^+\cdots[M^{III}(L4)(Solv)]^+$ dimers and they might be useful for estimations of the strength of such interactions in more magnetically complicated systems (*e.g.* with paramagnetic bridging complex, systems possessing magnetic ordering or slow-relaxation of magnetization).

## Acknowledgements

We acknowledge the financial support from the Czech Science Foundation (GAČR P207/11/0841), the Operational Program Research and Development for Innovations - European Regional Development Fund (CZ.1.05/2.1.00/03.0058) of the Ministry of Education, Youth and Sports of the Czech Republic, and Palacký University (PrF_2013_015 a 2014009.). The authors would like to thank Dr. Radka Křikavová for infrared spectroscopy measurements.

## Notes and references

[a] Regional Centre of Advanced Technologies and Materials & Department of Inorganic Chemistry, Faculty of Science, Palacký University, 17. listopadu 12,771 46, Olomouc, Czech Republic. Fax: +420585 634 954, E-mail: zdenek.travnicek@upol.cz.

† Footnotes should appear here. These might include comments relevant to but not central to the matter under discussion, limited experimental and spectral data, and crystallographic data.

*Electronic Supplementary Information (ESI) available: []. See DOI: 10.1039/b000000x*

[1] (a) C. Chappert, A. Fert, F. N. Van Dau, *Nat. Mater*., 2007, **6**, 813. (b) L. Bogani, W. Wernsdorfer, *Nat. Mater*., 2008, **7**, 179. (c) C. Felser, G. H. Fecher, B. Balke, *Angew. Chem., Int. Ed*., 2007, **46**, 668. (d) W. Wernsdorfer, *Nat. Nano,* 2009, **4**, 145.

[2] (a) V. H. Crawford, H. W. Richardson, J. R. Wasson, D. J. Hodgson, W. E. Hatfield, *Inorg. Chem.,* 1976, **15**, 2107. (b) J. Glerup, D. J. Hodgson, E. Pedersen, *Acta. Chem. Scand.,* 1983, **37**, 161. (c) S. M. Gorun, S. J. Lippard, *Inorg. Chem.,* 1991, **30**, 1625. (d) N. A. Law, J. W. Kampf, V. L. Pecoraro, *Inorg. Chim., Acta* 2000, **297**, 252.

[3] M. Ding, B. Wang, Z. Wang, J. Zhang, O. Fuhr, D. Fenske, S. Gao, *Chem. Eur. J.,* 2012, **18**, 915.

[4] (a) J. Larionova, S. A. Chavan, J. V. Yakhmi, A. G. Frøystein, J. Sletten, C. Sourisseau, O. Kahn, *Inorg. Chem.,* 1997, **36**, 6374. (b) O. Kahn, J. Larionova, J. V. Yakhmi, *Chem. Eur. J.,* 1999, **5**, 3443. (c) R. Herchel, J. Tuček, Z. Trávníček, D. Petridis, R. Zbořil, *Inorg. Chem.,* 2011, **50**, 9153.

[5] I. Nemec, M. Machata, R. Herchel, R. Boča, Z. Trávníček, *Dalton Trans.,* 2012, **41**, 14603.

[6] (a) E. Pardo, M. Verdaguer, P. Herson, H. Rousseliere, J. Cano, M. Julve, F. Lloret, R. Lescouezec, *Inorg. Chem.,* 2011, **50**, 6250. (b) I. Nemec, R. Herchel, I. Šalitroš, Z. Trávníček, J. Moncoľ, H. Fuess, M. Ruben, W. Linert, *CrystEngComm,* 2012, **14**, 7015. (c) M. Korabik, Z. Repická, L. Martiška, J. Moncol, J. Švorec, Z. Padělková, T. Lis, M. Mazúr, D. Valigura, *Z. anorg. allg. Chem*., 2011, **637**, 224. (d) D. Valigura, J. Moncol, M. Korabik, Z. Pučekova, T. Lis, J. Mrozinski, M. Melnik, *Eur. J. Inorg. Chem.,* 2006, 3813, (e) Z. Vasková, J. Moncoľ, M. Korábik, D. Valigura, J. Švorec, T. Lis, M. Valko, M. Melník, *Polyhedron*, 2010, **29**, 154-163, (f) B. Kozlevčar, N. Kitanovski, Z. Jagličić, N. A. G. Bandeira, V. Robert, B. Le Guennic, and P. Gamez, *Inorg.Chem*., 2012 **51** (5), 3094-3102, (g) J. S. Costa, N. A. G. Bandeira, B. Le Guennic, V. Robert, P. Gamez, G. Chastanet, L. Ortiz-Frade, and L. Gasque, *Inorg. Chem*., 2011 **50** (12), 5696-5705, (h) J. Tang, J. S. Costa, A. Golobič, B. Kozlevčar, A. Robertazzi , A. V. Vargiu , P. Gamez and J. Reedijk, *Inorg. Chem.*, 2009, **48** (12), 5473–5479.

[7] H. J. Buser, D. Schwarzenbach, W. Petter, A. Ludi, *Inorg. Chem.,* 1977, **16**, 2704.

[8] R. Lescouëzec, L. M. Toma, J. Vaissermann, M. Verdaguer, F. S. Delgado, C. Ruiz-Pérez, F. Lloret, M. Julve, *Coord. Chem. Rev.,* 2005, **249**, 2691.

[9] (a) R. Ishikawa, R. Miyamoto, H. Nojiri, B. K. Breedlove, and M. Yamashita, *Inorg. Chem.* 2013 **52** (15), 8300-8302, (b) H. Kara, A. Azizoglu, A. Karaoglu, Y. Yahsi, E. Gungor, A. Caneschi, L. Sorace, *CrystEngComm* 2012, **14**, 7320–7329, (c) H. Miyasaka, T. Madanbashi, A. Saitoh, N. Motokawa, R.Ishikawa, M. Yamashita, S. Bahr, W. Wernsdorfer, R. Clerac, *Chem. Eur. J.* 2012, **18**, 3942–3954, (d) X. Shen, Q. Zhang, H. Zhou, H. Zhou, A.Yuan, *New J. Chem.* 2012, **36**, 1180–1186, (e) E. Colacio, M. Ghazi, H. Stoeckli-Evans, F. Lloret, J. M. Moreno, C. Perez, *Inorg. Chem.,* 2001, **40**, 4876, (f) H. Z. Kou, J. K. Tang, D. Z. Liao, S. Gao, P. Cheng, Z. H. Jiang, S. P. Yan, G. L. Wang, B. Chansou, J. P. Tuchagues, *Inorg. Chem.,* 2001, **40**, 4839, (g) J. Larionova, M. Gross, M. Pilkington, H. Andres, H. Stoeckli-Evans, H. U. Gudel, S. Decurtins, *Angew. Chem. Int. Ed.,* 2000, **39**, 1605, (h) M. Ohba, N. Usuki, N. Fukita, H. Okawa, *Angew. Chem. Int. Ed.,* 1999, **38**, 1795, (i) Z. J. Zhong, H. Seino, Y. Mizobe, M. Hidai, A. Fujishima, S. Ohkoshi, K. Hashimoto, *J. Am. Chem. Soc.,* 2000, **122**, 2952, (j) A. Marvilliers, S. Parsons, E. Riviere, J. P. Audiere, M. Kurmoo, T. Mallah, *Eur. J. Inorg. Chem.,* 2001,1287.

[10] (a) M. Ohba, H. Okawa, *Coord. Chem. Rev.,* 2000, **198**, 313. (b) M. Verdaguer, A. Bleuzen, V. Marvaud, J. Vaissermann, M. Seuleiman, C. Desplanches, A. Scuiller, C. Train, R. Garde, G. Gelly, C. Lomenech, I. Rosenman, P. Veillet, C. Cartier, F. Villain, *Coord. Chem. Rev.,* 1999, **190**, 1023. (c) W. P. Fehlhammer, M. Fritz, Chem. Rev. 1993, 93, 1243; d) K. R. Dunbar, R. A. Heintz, *Prog. Inorg. Chem.,* 1997, **45**, 283. (e) S. M. Holmes, G. S. Girolami, *J. Am. Chem. Soc.,* 1999, **121**, 5593. (f) L. G. Beauvais, J. R. Long, *J. Am. Chem. Soc.,* 2002, **124**, 12096. (g) O. Sato, T. Iyoda, A. Fujishima, K. Hashimoto, *Science,* 1996, **272**, 704. (h) T. D. Harris, H. S. Soo, C. J. Chang, J. R. Long, *Inorg. Chim. Acta,* 2011, **369**, 91.

[11] (a) H. J. Choi, J. J. Sokol, J. R. Long, *Inorg. Chem.,* 2004, **43**, 1606. (b) P. Przychodze, M. Rams, C. Guyard-Duhayon, B. Sieklucka, *Inorg. Chem. Commun.,* 2005, **8**, 350. (c) M. Ferbinteanu, H. Miyasaka, W. Wernsdorfer, K. Nakata, K. Sugiura, M. Yamashita, C. Coulon, R. Clerac, *J. Am. Chem. Soc.,* 2005, **127**, 3090. (d) H. S. Yoo, H. H. Ko, D. W. Ryu, J. W. Lee, J. H. Yoon, W. R. Lee, H. C. Kim, E. K. Koh, C. S. Hong, *Inorg. Chem.,* 2009, **48**, 5617. (e) H. Y. Kou, Y. N. Ni, B. C. Zhou, R. J. Wang, *Inorg. Chem. Commun.,* 2004, **7**, 1150. (f) F. Tuyčras, A. Schiller, C. Duhayon, M. Hernandez-Molina, F. F. de Biani, M. Verdaguer, T. Mallah, W. Wernsdorfer, V. Marvaud, *Inorg. Chim. Acta,* 2008, **361**, 3505. (g) M. Atanasov, C. Busche, P. Comba, F. E. Hallak, B. Martin, G. Rajaraman, J. van Slageren, H. Wadepohl, *Inorg. Chem.,* 2008, **47**, 8112.

[12] $H_2L4a$ = *N,N′*-cyklohexane-bis(salicylideneiminate), $H_2L4b$ = *N,N′*-benzene-bis(salicylideneiminate), $H_2L4c$ = *N,N'*-ethylene-bis(3-ethoxysalicylideneiminate), $H_2L4d$ = *N,N'*-1-methylethylene-bis(3-ethoxysalicylideneiminate), $H_2L4e$ = *N,N′*-benzene-bis(naphthylide neiminate), $H_2L4f$ = *N,N'*-ethylene-bis(salicylideneiminate), $H_2L4g$ = *N,N′*-1-methylethylene- bis(salicylideneiminate), $H_2L4h$ = *N,N′*-1,1,2,2-tetramethyl etylene-bis(salicylideneiminate), $H_2L4i$ = *N,N'*-ethylene-bis(3-methoxysalicylideneiminate), $H_2L4j$ = *N,N'*-ethylene-bis(5-bromosalicylideneiminate), $H_2L4k$ = *N,N′*-1,3-propylene-bis(5-bromo salicylideneiminate), $H_2L4l$ = *N,N'*-1,3-propylene -bis(3-methoxy salicylideneiminate), $H_2L4m$ = *N,N′*-1,1,2,2-tetramethylethylene-bis(naphthylideneiminate), $H_2L4n$ = *N,N′*-benzene-bis(4-aminodiethylenesalicylideneiminate), $H_2L4$ o = *N,N′*-3-methylbenzene-bis(3-ethoxysalicylideneiminate) and $H_2L4p$ = *N,N′*-ethylene-bis(salicylidenebenzeneiminate).

[13] (a) R. Dreos, G. Nardin, L. Randaccio, P. Siega, G. Tauzher, V. Vrdoljak, *Inorg. Chim. Acta,* 2003, **349**, 239. (b) R. Blaauw, J. L. van der Baan, S. Balt, M. W. G. de Bolster, G. W. Klumpp, H. Kooijman, A. L. Spek, *Chem. Commun.,* 1998, 1295. (c) B. C. Wang, B. T. Huie, W. P. Schaefer, *Acta Crystallogr. Sect. B: Struct. Crystallogr. Cryst. Chem.,* 1979, **35**, 1232. (d) R. Dreos, G. Nardin, L. Randaccio, P. Siega, G. Tauzher, V. Vrdoljak, *Inorg. Chem.,* 2003, **42**, 6805. (e) R. Blaauw, I. E. Kingma, J. H. Laan, J. L. van der Baan, S. Balt, M. W. G. de Bolster, G. W. Klumpp, W. J. J. Smeets, A. L. Spek, *J. Chem. Soc., Perkin Trans.,* 2000, **1**, 1199. (f) J. Welby, L. N. Rusere, J. M. Tanski, L. A. Tyler, *Inorg. Chim. Acta,* 2009, **362**, 1405. (g) S. Bruckner, M. Calligaris, G. Nardin, L. Randaccio, *Acta Crystallogr., Sect. B: Struct. Crystallogr. Cryst. Chem.,* 1969, **25**, 1671.

[14] (a) A. Geiss, H. Vahrenkamp, *Eur. J. Inorg. Chem.,* 1999, 1793. (b) C. H. Yang, J. A. Ladd, V. L. Goedken, *J. Coord. Chem.,* 1988, **19**, 235. (c) M. Gerloch, F. E. Mabbs, *J. Chem. Soc. A,* 1967, 1900. (d) J. L. Resce, J. C. Fanning, C. S. Day, S. J. Uhm, A. F. Croisy, L. K. Keefer, *Acta Crystallogr., Sect. C: Cryst. Struct. Commun.,* 1987, **43**, 2100. (e) E. Evangelio, N. P. Rath, L. M. Mirica, *Dalton Trans.,* 2000, **41**, 8010.

[15] C. Y. Wong, W. L. Man, C. Wang, H. L. Kwong, W. Y. Wong, T. C. Lau, *Organometallics,* 2008, **27**, 324.

[16] J. M. McInnes, D. Swallow, A. J. Blake, P. Mountford, *Inorg. Chem.,* 1998, **37**, 5970.

[17] (a) M. Odoko, N. Tsuchida, N. Okabe, *Acta Crystallogr., Sect. E: Struct. Rep. Online,* 2006, **62**, m708. (b) N. Meyer, P. W. Roesky, *Z. Anorg. Allg. Chem.,* 2007, **633**, 2292. (c) H. Kooijman, A. L. Spek, M. Kuil, P. W. N. M. van Leeuwen, *Private Communication,* 2011.

[18] (a) R. J. Tao, C. Z. Mei, B. T. Liu, J. Y. Niu, *Chin. J. Chem.,* 2006, **24**, 1559. (b) M. M. Bhadbhade, D.Srinivas, *Inorg. Chem.,* 1993, **32**, 6122.

[19] Y. Ding, Z. Ku, L. Wang, Y. Hu, Y. Zhou, *Acta Crystallogr., Sect. E: Struct. Rep. Online,* 2008, **64**, m173.

[20] I. Nemec, T. Šilha, R. Herchel, Z. Trávníček, *Eur. J. Inorg. Chem.,* 2013, 5781.

[21] T. Šilha, I. Nemec, R. Herchel, Z. Trávníček, *CrystEngComm,* 2013, **15**, 5351.

[22] M. Clemente-León, E. Coronado, J. R. Galán-Mascarós, C. J. Gómez-García, T. Woike,J. M. Clemente-Juan, *Inorg. Chem.,* 2001, **40**, 87.

[23] C. Yang, Q. Wang, Y. Ma, G. Tang, D. Liao, S. Yan, G. Yang,P. Cheby, *Inorg. Chem.,* 2010, **49**, 2047.

[24] R. Ababei, Y. Li, O. Roubeau, M. Kalisz, N. Bréfuel, C. Coulon, E. Harté , X, Liu, C, Mathoniére, R. Clérac, *New J. Chem.,* 2009, **33**, 1237.

[25] T. Wang, J. Xie, C. Xia, Y. Wu, J. Jing, J. Huaxue, *Chin. J. Struct. Chem.,* 2010, **29**, 1265.

[26] M. Clemente-León, E. Coronado, J. R. Galán-Mascarós, C. J. Gómez-García, Th. Woike, J. M. Clemente-Juan, *Inorg. Chem.,* 2001, **40**, 87.

[27] A. Yuan, L. Lu, X. Shen, K. Yu, *Transition Met. Chem.,* 2003, **28**, 163.

[28] X. Shen, Z. Xu, A. Juan, Z. Huang, *Transition Met. Chem.,* 2004, **29**, 100.

[29] (a) N. A. G. Bandeira, B. Le Guennic, *J. Phys. Chem., A* 2012, **116**, 3465. (b) C. Desplanches, E. Ruiz, A. Rodriguez-Fortea, S. Alvarez, *J. Am. Chem. Soc.,* 2002, **124**, 5197. (c) B. Le Guennic, N. Ben Amor, D. Maynau, V. Robert, *J. Chem. Theory Comput.,* 2009, **5**, 1506.

[30] R. Pritchard, S. A. Barrett, C. A. Kilner, M. A. Halcrow, *Dalton Trans.,* 2008, 3159.

[31] K. Nakamoto, Infrared and Raman Spectra of Inorganic and Coordination Compounds, Part B: Applications in Coordination, Organometalic and Bioinorganic Chemistry, fifth ed., Willey, New York, 1997.

[32] The standard deviations were calculated as $\sigma_i = (P_{ii}^{-1} \cdot S/(N-k))^{-1/2}$, where $P_{ij} = \Sigma(\delta\mu_n/\delta a_i \cdot \delta\mu_n/\delta a_j)$ and $S = \Sigma(\mu_n - \mu_n^{exp})^2$ with $n = 1$ to $N$; $a_i$ and $a_j$ are fitted parameters, $N$ is number of experimental points (sum of temperature and field dependent data), $\mu_n$ and $\mu_n^{exp}$ are the calculated and experimental effective magnetic moments for given temperature and magnetic field. The $\sigma_i$ was then multiplied by

Student's $t_{95\%}$ to provide confidence limits with 95% probabilities listed in text.
[33] R. Boča, Coord. *Chem. Rev.,* 2004, **248**, 757.
[34] CrysAlis CCD and CrysAlis RED, Version 1.171.33.52, Oxford Diffraction Ltd., England, 2009.
[35] G. M. Sheldrick, *Acta Crystallogr., Sect., A* 2008, **64**, 112.
[36] (a) C. Lee, W. Yang, R. G. Parr, *Phys. Rev. B* 1988, **37**, 785. (b) A. D. Becke, *J. Chem. Phys.,* 1993, **98**, 1372. (c) A. D. Becke, *J. Chem. Phys.,* 1993, **98**, 5648. (d) P. J. Stephens, F. J. Devlin, C. F. Chabalowski, M. J. Frisch, *J. Phys. Chem.,* 1994, **98**, 11623.
[37] (a) E. Ruiz, J. Cano, S. Alvarez, P. Alemany, *J. Comput. Chem.*, 1999, **20**, 1391. (b) E. Ruiz, A. Rodríguez-Fortea, J. Cano, S. Alvarez, P. Alemany, *J. Comput. Chem. ,*2003, **24**, 982.
[38] (a) K. Yamaguchi, Y. Takahara, T. Fueno, in: V. H. Smith (Ed.), Applied Quantum Chemistry, Reidel, Dordrecht, 1986, p. 155. (b) T. Soda, Y. Kitagawa, T. Onishi, Y. Takano, Y. Shigeta, H. Nagao, Y. Yoshioka, K. Yamaguchi, *Chem. Phys. Lett.,* 2000, **319**, 223.
[39] (a) A. Schaefer, H. Horn,R. Ahlrichs, *J. Chem. Phys.,* 1992, **97**, 2571. (b) A. Schafer, C. Huber, R. J. Ahlrichs, *Chem. Phys.,* 1994, **100**, 5829. (c) F. Weigend,R. Ahlrichs, *Chem. Phys.,* 2005, **7**, 3297.
[40] A. Pantazis, X. Y. Chen, C. R. Landis, F. Neese, *J. Chem. Theory Comput.,* 2008, **4**, 908.
[41] (a) F. Neese, F. Wennmohs, A. Hansen, U. Becker, *Chem. Phys.,* 2009, **356**, 98. (b) R. Izsak, F. Neese, *J. Chem. Phys.,* 2011, **135**, 144105.
[42] (a) A. D. Becke, *Phys. Rev. A* ,1988, **38**, 3098. (b) J. P. Perdew, *Phys. Rev. B,* 1986, **33**, 8822. (c) J. P. Perdew, *Phys. Rev. B* ,1986, **34**, 7406.
[43] S. Sinnecker, A. Rajendran, A. Klamt, M. Diedenhofen, F. Neese, *J. Phys. Chem., A* 2006, **110**, 2235.
[44] (a) S. Grimme, *J. Comput. Chem.,* 2004, **25**, 1463. (b) S. Grimme, *J. Comput. Chem.,* 2006, **27**, 1787. (c) S. Grimme, J. Antony, S. Ehrlich, H. Krieg, *J. Chem. Phys.,* 2010, **132**, 154104.

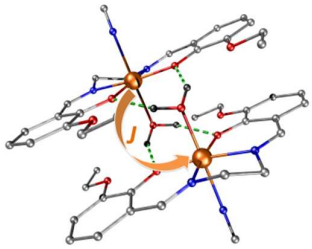


The detailed investigations of the magnetic coupling and magnetic anisotropy in a series of Schiff base salen-like Fe(III) and Mn(III) complexes, based on SQUID experiments and DFT calculations, are reported.